Nanoscale

REVIEW

View Article Online
View Journal | View Issue

Check for updates

Cite this: *Nanoscale*, 2023, **15**, 3051

# Toward a new generation of permeable skin electronics

Jiawei Yang,[a,b] Zongman Zhang,[a] Pengcheng Zhou,[a] Yujie Zhang,[a,b] Yi Liu,[a,b] Yumiao Xu,[a] Yuheng Gu,[a] Shenglin Qin,[a] Hossam Haick *[c] and Yan Wang *[a,b,d]

Received 7th November 2022,
Accepted 2nd January 2023

DOI: 10.1039/d2nr06236d

rsc.li/nanoscale

Skin-mountable electronics are considered to be the future of the next generation of portable electronics, due to their softness and seamless integration with human skin. However, impermeable materials limit device comfort and reliability for long-term, continuous usage. The recent emergence of permeable skin-mountable electronics has attracted tremendous attention in the soft electronics field. Herein, we provide a comprehensive and systematic review of permeable skin-mountable electronics. Typical porous materials and structures are first highlighted, followed by discussion of important device properties. Then, we review the latest representative applications of breathable skin-mountable electronics, such as bioelectrical sensors, temperature sensors, humidity and hydration sensors, strain and pressure sensors, and energy harvesting and storage devices. Finally, a conclusion and future directions for permeable skin electronics are provided.

Published on 03 oajagemánnu 2023. Downloaded on 2026-05-06 16:33:29.

## 1. Introduction

Flexible electronic devices have received significant attention for their wide range of applications in recent years. They have been gradually moving towards miniaturization and 'true' wearability through innovative material and structure design. As the largest organ of the human body, human skin has many intrinsic characteristics, such as excellent mechanical properties and tactile sensing capabilities.[1,2] Electronic devices attached directly to human skin, *i.e.*, skin-mountable electronics, also known as skin electronics, have been designed by mimicking skin functionalities. Such devices can perceive a person's internal state and/or external environment and convey information to the user. Skin-mountable electronics are considered to be one of the most important directions of next-generation wearable electronics.[3–5] To date, great efforts have been made to develop high-performance skin-mountable electronics, such as temperature sensors,[6] energy harvesting and storage devices,[7,8] actuators and displays.[9,10]

From the perspective of physiological requirements, healthy skin is always in a stable microenvironment that ensures effective sweat drainage. Non-permeable skin-mountable electronics can cause skin inflammation or irritation after long-term attachment. Furthermore, the resulting sweat accumulation leads to low-quality bio-signal acquirement.[11] In the past three decades, the development of skin-mountable electronics has mainly focused on enhancing mechanical and sensing properties, while gas permeability has been often neglected. Most existing skin-mountable electronics are composed of impermeable materials with thick film-based or bulky layered structures.[12–14] For long-term applications, *e.g.*, disease prevention,[15,16] screening,[17] diagnosis,[18,19] and treatment,[20–22] skin-mountable electronics need to be breathable, *i.e.*, gas-permeable. Breathable skin-mountable electronics were reported by Rogers's group in 2014.[23] Such developed breathable skin-mountable electronics can realize the continuous, long-term collection of high-fidelity bioelectrical, biochemical, and biophysical information.[23,24]

Together with advanced material and structure design, various breathable skin-mountable electronics have been reported, such as bioelectrical sensors,[25] temperature sensors,[26] humidity and hydration sensors,[27] strain and pressure sensors,[28] and energy harvesting and storage devices.[29] Fig. 1 shows the development of representative examples in recent years. In terms of breathable soft electronics, the existing reviews have been focused on triboelectric

[a]*Department of Chemical Engineering, Guangdong Technion-Israel Institute of Technology (GTIIT), Shantou, Guangdong 515063, China. E-mail: yan.wang@gtiit.edu.cn*
[b]*Department of Chemical Engineering, Technion-Israel Institute of Technology (IIT), Haifa 3200003, Israel*
[c]*Department of Chemical Engineering and Russell Berrie Nanotechnology Institute, Technion-Israel Institute of Technology, Haifa 3200003, Israel. E-mail: hhossam@technion.ac.il*
[d]*Guangdong Provincial Key Laboratory of Materials and Technologies for Energy Conversion, Guangdong Technion-Israel Institute of Technology, Shantou, Guangdong 515063, China*

Published on 03 oajagemánnu 2023. Downloaded on 2026-05-06 16:33:29.

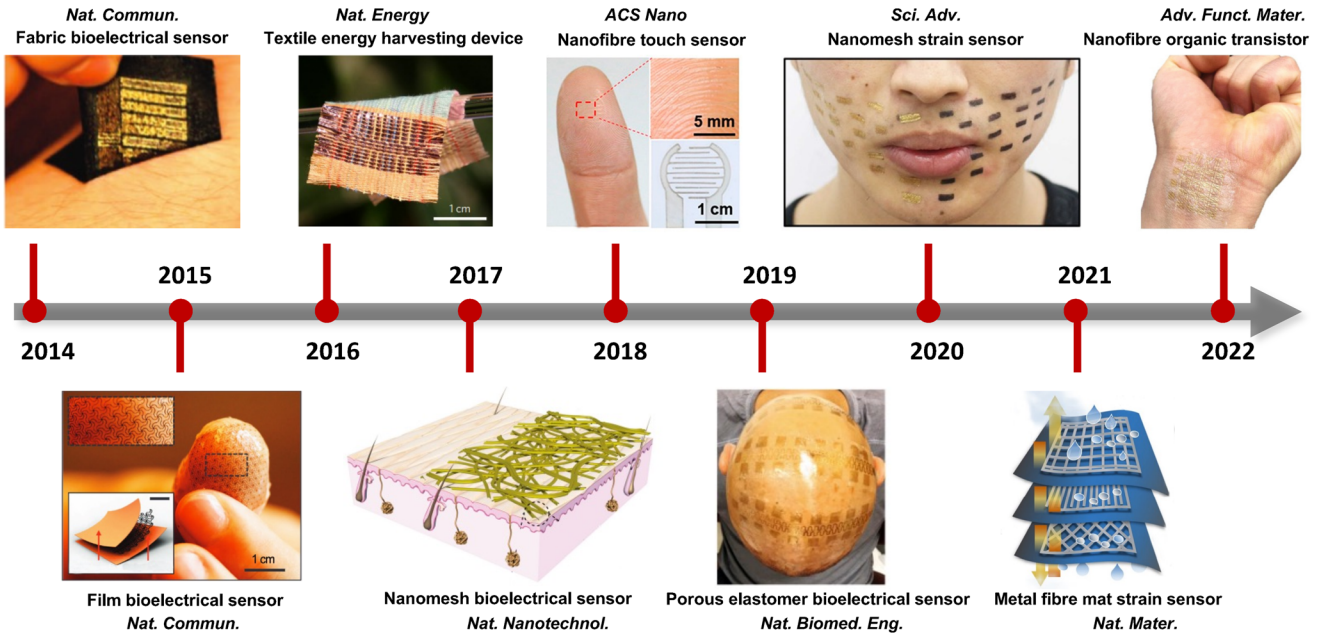


**Fig. 1** Representative examples of advanced breathable skin-mountable electronics (2014–2022). Reproduced with permission from ref. 23, 39–46 Copyright 2014, 2015, 2016, 2017, 2019, 2021 Nature Publishing Group; 2018 American Chemical Society; 2020 American Association for the Advancement of Science; 2022 Wiley-VCH.

electronics,[30] electrospun nanofibre-based soft electronics,[31] paper-based wearable electronics,[32] permeable conductors,[33] fibre-based electronics,[34–36] textile-based electronics[37] and breathable electronics for physiological signal monitoring.[38] Recently, Huang *et al.* summarized critical metrics and design strategies towards permeable electronics.[24] However, there lacks a comprehensive and systematic review on breathable skin-mountable electronics discussing all aspects of materials and structures, device properties, and applications. Here, we provide a bird's eye view of the latest advancements in breathable skin-mountable electronics by summarizing typical porous materials and structures, device properties, and applications. We further discuss current challenges and pertinent solutions in this field to boost future continuous development.

**Yan Wang**

*Yan Wang joined the Guangdong Technion-Israel Institute of Technology as an Associate Professor in Nov. 2021. She received her Ph.D. degree majoring in Chemical Engineering from Monash University in 2018 and completed her postdoc training at the Department of Electrical and Electronic Engineering, The University of Tokyo. In the soft electronics field, Dr Yan Wang has published over 30 scientific articles in flagship journals like* Science, Nat. Electron., Sci. Adv., PNAS, ACS Nano, Chem. Soc. Rev., etc. *Her research works have been featured in renowned media, such as CNN, Science, Nature Materials, Australia SBS evening news, and Nikkan Kogyo Shimbun. At Guangdong Technion, her research group mainly focuses on materials development and the practical implementation of soft wearables in real-life situations towards ambulatory health care and the Internet of Things.*

## 2. Material and structure strategy

For device development, material and structure strategies play a decisive role in the performance and applications of breathable skin-mountable electronics. In the past few years, significant efforts have been made to design unconventional porous materials and structures for high-performance breathable skin-mountable electronics. Here, we summarize four approaches: ultrathin materials and devices, electrospun nanofibre-based, yarn/fabric-based, and structure design (Fig. 2).

### 2.1. Ultrathin materials and devices

The excessive thickness of skin-mountable electronics can limit permeability, thus affecting long-term health monitoring. To achieve breathability, one typical strategy is to fabricate ultrathin materials and devices. In general, ultrathin materials and devices include free-standing conductive membranes, metallic meshes, and electronic tattoos from carbon-based materials.

Free-standing ultrathin conductive membranes are usually made from conductive polymer membranes and hybrid nano-

 This journal is © The Royal Society of Chemistry 2023

Published on 03 oajagemännu 2023. Downloaded on 2026-05-06 16:33:29.

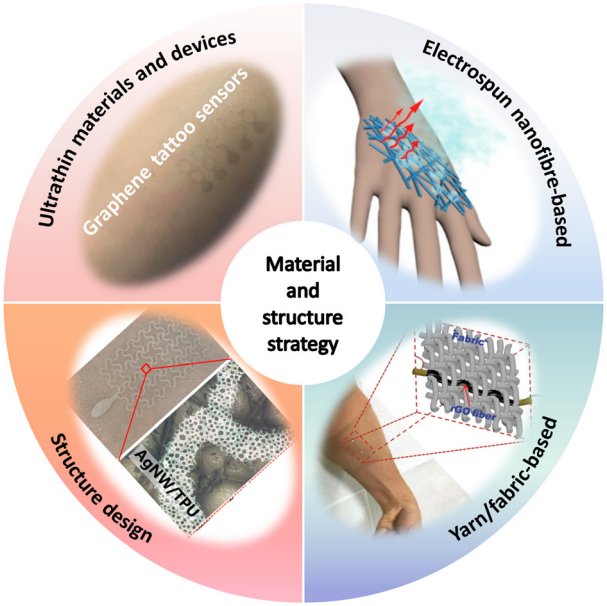


**Fig. 2** Four approaches to material and structure strategy for breathable skin-mountable electronics. Reproduced with permission from ref. 50–53. Copyright 2020 Elsevier; 2021, 2020 American Chemical Society; 2018, 2019 Wiley-VCH.

films. In the past two decades, conductive polymers have attracted great interest in skin-mountable electronics due to their unique properties (*e.g.*, light weight, flexibility, stretchability, and corrosive resistivity) and a variety of co-tailored features to suit specific needs. Among the various polymeric conductive materials, poly(3,4-ethylenedioxythiophene):polystyrene sulfonate (PEDOT:PSS) is considered to be one of the most popular and widely studied materials.[47] As for breathable ultrathin polymer membranes, a typical example is ultrathin skin-mountable electrodes with a sub-micron structure. The hybrid electrodes are composed of a silver nanowires (AgNWs) network and conductive polymer films. By depositing AgNWs on PEDOT:PSS, the PEDOT:PSS/AgNWs hybrid electrode had an ultrathin structure (230 nm) and excellent gas permeability (Fig. 3a and b). It exhibited lower impedance than that of commercial gel electrodes and superior signal acquisition capabilities for ECG and EMG.[48] Free-standing hybrid nanofilms have also been developed as breathable skin-mountable electronics.[44,49] For example, Wang *et al.* reported robust, self-adhesive, permeable nanofilms with an ultrathin thickness (95 nm). The fabrication process is shown in Fig. 3c, where the hybrid breathable nanofilms were prepared by a simple dip-coating technique. The polyurethane (PU)/polydimethylsiloxane (PDMS) nanofilms had strong adhesion properties and directly adhered to human skin. The thinness geometry and great skin compliance were confirmed by scanning electron microscope (SEM) and optical images (Fig. 3d). The Au-coated nanofilm dry electrodes enabled continuous monitoring of human physiological signals for up to 1 week with high signal-to-noise ratio (SNR) (34 dB).[49] Wang *et al.* also developed an ultrathin (only 430 ± 18 nm) nanomesh strain gauge with excellent gas permeability (Fig. 3e). The strain sensor exhibited impressive mechanical durability of 5000 cycles stretch/release under 60% strain. Nanomesh sensors were successfully used to evaluate strain mapping of facial skin deformation during speech, and the results were compared with thin-film PDMS samples. It was demonstrated that the gas-permeable device had minimal mechanical interference with the facial skin during speech. The skin-attached strain sensors moved naturally with dynamic skin deformations (Fig. 3f). This excellent consistency originated from the thin and porous geometry, ultralight weight, and softness of the device.[44]

Freestanding ultrathin metallic meshes have been developed as breathable skin-mountable electronics due to their great conductivity, low skin–electrode impedance, and ease of fabrication.[54] For example, Xu *et al.* used a low-cost method to fabricate a lightweight freestanding $MnO_2$–Au–Ni mesh electrode. A two-step electrodeposition process was introduced to deposit the $MnO_2$–Au on the Ni-reticulated electrode. The hybrid $MnO_2$–Au–Ni electrode exhibited an excellent air permeability of 2600 mm $s^{-1}$ at 10 Pa and a thickness of only 6 μm. The as-assembled all-solid-state supercapacitor had a great optical transparency (86%) and withstood varying degrees of deformation (*e.g.*, bending, crumpling and folding).[55] Li *et al.* reported a novel ultrathin (10 μm) permeable sensor for glucose monitoring. The non-enzymatic glucose sensor was fabricated by *in situ* growth of Cu nanoparticles on a Ni electrode. The sensor showed an extremely low detection limit (2 μM) and superior sensitivity (8.51 mA $cm^{-2}$ $mM^{-1}$).[56] Besides, metal nanowire percolation networks are promising electrodes components, including AgNWs network electrodes[57–61] and CuNWs electrodes.[62–66] Their ultra-thin thickness, porosity, and high conductivity demonstrate great potential for developing gas-permeable skin-mountable electronics.

Carbon-based electronic tattoos, such as graphene-based, have been utilized to prepare breathable skin-mountable electronics.[67,68] These devices showed great skin compliance and excellent electrical conductivity, and hold great promise for high-fidelity health monitoring. For instance, Ameri *et al.* reported ultrathin graphene multimode electronic tattoos (463 ± 30 nm) (Fig. 3g). The tattoos exhibited optical transparency of 85%, stretchability of over 40% strain, and impressive permeability (Fig. 3h). As dry electrodes, these electronic tattoos can be directly attached to human skin for ECG, EMG, and EEG monitoring.[53] Kireev *et al.* reported breathable graphene electronic tattoo sensors with low interface impedance (6.8 ± 0.6 kΩ at 10 kHz). Porous structures were introduced to the graphene tattoos to achieve a breathability of 2770 ± 494 g $m^{-2}$ $d^{-1}$. The breathable electronic tattoos were further utilized as skin-mountable electronic heaters, demonstrating excellent heating efficiency (6 mW $°C^{-1}$).[13]

### 2.2. Electrospun nanofibre-based

Electrospun nanofibres provide an excellent building block for the development of breathable skin-mountable electronics. This is because nanofibre mats prepared by the electro-

Published on 03 oajagemánnu 2023. Downloaded on 2026-05-06 16:33:29.

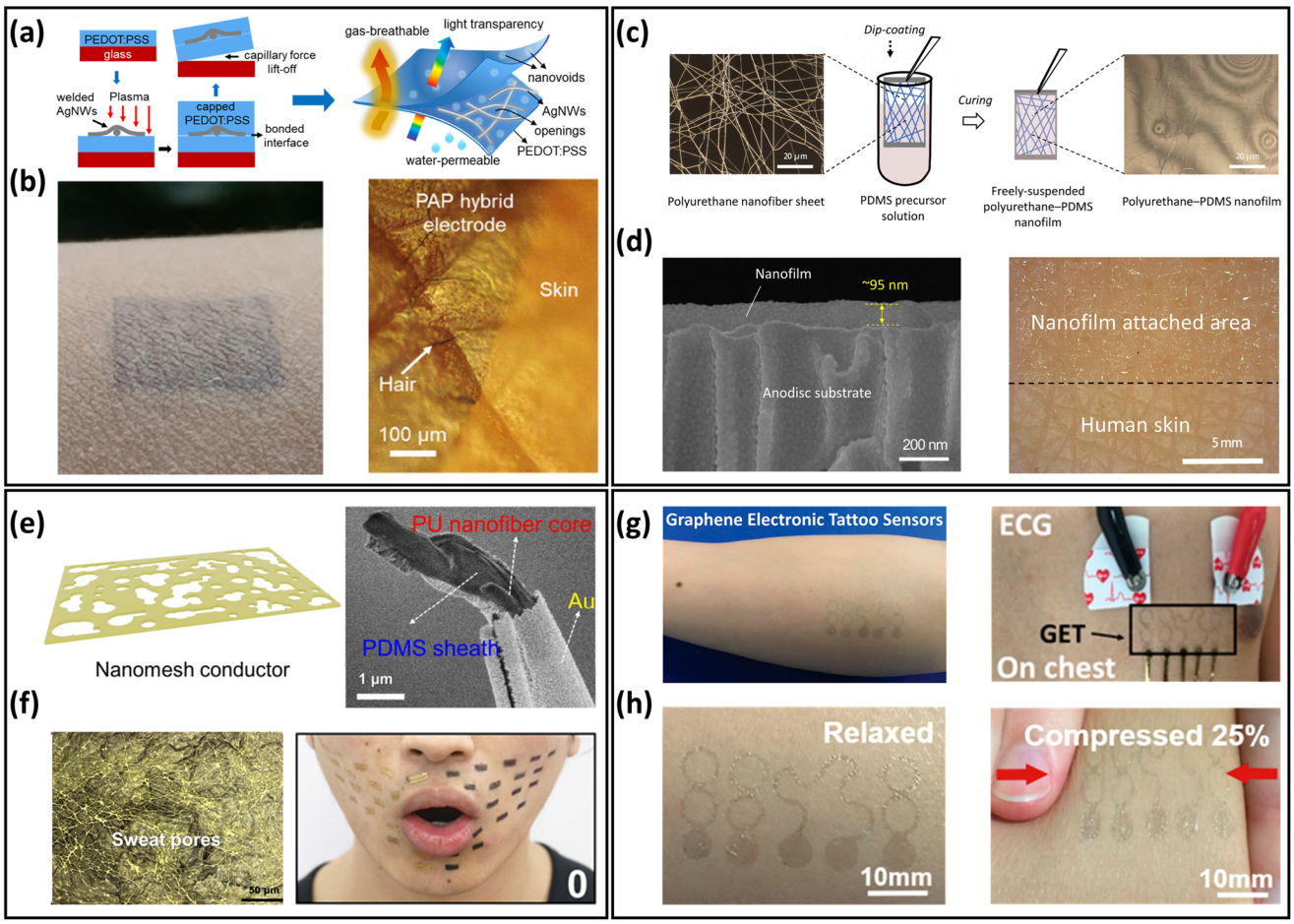


**Fig. 3** Ultrathin materials and devices of breathable skin-mountable electronics. (a) Schematic diagram of the manufacturing process for freestanding PAP hybrid electrodes. (b) Optical images of PAP hybrid electrodes attached to human skin. Reproduced with permission from ref. 48. Copyright 2020 American Chemical Society. (c) Schematic diagram of the fabrication of polyurethane–PDMS nanofilms. (d) SEM images of a cross-section of a nanofilm attached on the anodisc substrate and an image of nanofilm applied to the back of a hand. Reproduced with permission from ref. 49. Copyright 2022 National Academy of Sciences. (e) Schematic and SEM image of PU-PDMS nanomesh conductors. (f) Microscopic image of the device on the fingertip replica and photograph of a face during speech of "O". Reproduced with permission from ref. 44 Copyright 2020 American Association for the Advancement of Science. (g) Schematic of the graphene electronic tattoo sensor. (h) Graphene electronic tattoo mounted on skin and its compressed image. Reproduced with permission from ref. 53. Copyright 2017 American Chemical Society.

spinning technique tend to have large porosity and surface area, as well as superior mechanical flexibility.[69–71] Most electrospinnable materials are organic polymers in solution or melt forms.[72] To date, there are over 100 organic polymers that can directly produce nanofibres through solution electrospinning. Typical polymers include polyvinyl alcohol (PVA),[73] PU,[74,75] thermoplastic polyurethane (TPU),[76] polystyrene (PS),[77] poly(vinylidene fluoride) (PVDF),[78] poly(vinyl chloride) (PVC),[79] *etc.* A large number of gas-permeable skin-mountable electronics have been developed using the electrospun nanofibre-based approach on such polymer materials.[31,73,80,81] Here, we will discuss electrospun nanofibres as the sacrificial layer and/or the support scaffold layer for preparing breathable skin-mountable electronics.

A typical example is gas-permeable, inflammation-free nanomesh on-skin sensors fabricated by Miyamoto *et al.*[41] PVA nanofibres were first fabricated by electrospinning, and then Au layers were deposited on them using shadow masks. As PVA is water-soluble, the substrate-free Au nanomesh conductor was successfully attached to human skin, and the thickness of the prepared Au layer was only 70–100 nm (Fig. 4a). Compared with traditional flat substrates, the nanomesh had good adhesion to human skin. And due to its excellent air permeability and great biocompatibility, it can meet the requirements of long-term use. By depositing a thin layer of metals (*e.g.*, Au, Cu, Ag, and Al) on PVA electrospun nanofibre mats by vacuum deposition, Wu *et al.* fabricated transparent metal nanotrough networks. After dissolving the PVA electrospun mat template, the transparent metal nanotrough networks can be firmly attached to various substrates (plastic films and papers). SEM images showed a thickness of only 400 nm (Fig. 4b). The nanofibres used as sacrificial layers have thin thickness and porous structure, thus providing the basis for permeable skin-mountable electronics.[71]

 This journal is © The Royal Society of Chemistry 2023

Published on 03 oajagemánnu 2023. Downloaded on 2026-05-06 16:33:29.

Besides sacrificial layers, electrospun nanofibres can be fabricated as supporting scaffolds to prepare breathable skin-mountable electronics.[82,83] Customized depositions of conductive materials on the fibres enhance the conductivity and detection limits of the sensors. For example, Fan *et al.* fabricated a scaffold-reinforced conductive nanonetwork by electrospinning. Using vacuum filtration, solution-dispersed AgNWs penetrated polyamide nanofibre scaffolds (Fig. 4c). The nanofibres have an average diameter of 80 nm and form a continuous network. The assembled breathable epidermal electrodes showed great light transmission (84.9%) and excellent skin adhesion (Fig. 4d). The fibrous device with excellent permeability can be utilized as a touch sensor with a low sheet resistance of 8.2 Ω $sq^{-1}$.[42] Another example is the nanomesh elastic strain sensor made by Jiang *et al.* It was composed of PU nanofibres and AgNWs. The morphology of randomly interconnected AgNWs on PU nanofibres could be observed by SEM images. The average diameters of AgNWs and PU nanofibres were 153 nm and 0.74 μm, respectively (Fig. 4e). The porous strain sensor presented impressive electrical conductivity (9190 S $cm^{-1}$), superior stretchability (310% strain), and great mechanical durability (1000 cycles under 70% strain). Besides, the elastic conductors had an excellent water vapor transmission rate (WVTR) of 9.6 mg $cm^{-2}$ $h^{-1}$, which was attributed to the porous nanostructures (Fig. 4f).[84]

Furthermore, layered strategies have been applied by many research groups to fabricate all-fibre-based breathable skin-mountable electronics, such as acoustic sensors,[85] triboelectric nanogenerators (TENG),[86,87] strain and pressure sensors,[88,89] and temperature sensors, *etc.*[90,91]

### 2.3. Yarn/fabric-based

As a composite unit of textiles, yarn/fabric has obvious porous characteristics and is widely utilized in breathable skin-mountable electronics.[92,93] Excellent breathability can be obtained by creating gaps among fibrous weaving. Also, based on the yarn structure, sensor-based yarn/fabric can be easily integrated into garments.[94] In summary, yarn/fabric-based breathable skin-mountable electronics can be prepared in several ways, such as weaving, knitting, stitching, embroidery, nonwoven, and printing (Fig. 5). Each fabrication technique has unique advantages, and its outstanding mechanical flexibility and highly integrated structure integration can provide novel materials and device solutions for exploring gas-permeable skin-mountable electronics.

Yarns or fabrics have been widely used as supporting materials due to their flexibility and machinability.[95,96] Using coating techniques, conductive materials such as carbon nanotubes (CNTs) fabrics,[97] graphene textiles,[98] and AgNWs fabrics[99] can be deposited on the surface of fabrics or yarns. A representative example is the silk sericin-assisted washable electronic textile. A scalable and facile dyeing process was used to make a uniform and stable sericin-decorated graphene. SEM images revealed that the graphene textiles were composed of several loop-structured yarns. Also, the breathability of the fabric was demonstrated by measuring the WVTR on the textile. It exhibited a similar WVTR to that of the pristine textile ($p > 0.05$). The combination of hydrophilicity and breathability allowed the fabric to wick away perspiration quickly and improved wearing comfort. Furthermore, the porous textiles can be fabricated as bioelectrical sensors for EMG monitoring. These sensors were built into a fully textured multimode system to perform complex human motion recognition.[100] Liu *et al.* reported a yarn-based strain sensor made by polymer-assisted metal deposition and *in situ* Cu growth on viscose yarn. After the removal of the PVA substrate, the continuous conductive yarns formed a strain-sensing network with huge sensitivity (Gauge Factor (GF) = 49.5). In particular, the yarn-based sensor exhibited remarkable permeability (air and WVTR was over 1500 L $m^{-2}$ $s^{-1}$ and 25 g $m^{-2}$ $h^{-1}$, respectively) due to pore channels. The strain sensor showed accurate perception of small body movements such as chewing, throat vibration, and breathing. Based on its great sensitivity, wide sensing range (0–100 kPa), and remarkable breathability, it can be successfully utilized to monitor full-range human body movements.[101]

The direct spinning method is widely applied to prepare high-performance yarn-based breathable skin-mountable electronics. Typical spinning methods include ring-spinning,[108] rotor-spinning,[109] twisting,[110,111] wrap-spinning,[112] and core-spinning.[113,114] Among these methods, twisting is an effective and popular way of enhancing the cohesion between yarns. For example, Zhang *et al.* fabricated Fermat-spiral-based energy yarns (FSBEY) electrodes with improved dynamic structural stability. FSBEY electrodes were composed of core stretchable spandex yarn electrodes and sheathed dielectric PVDF nanofibres. Firstly, the stretchable yarns were made by wrapping spandex with conductive fibres using a fast-speed braiding machine. Then the PVDF-trifluoroethylene nanofibres were twisted on the surface of the pre-stretched core yarn using the conjugated electrospinning technique. The stretchable electrodes exhibited great stretchability (200% strain), high conductivity (298 S $cm^{-1}$), and excellent breathability (0.024 g $cm^{-2}$ $h^{-1}$). FSBEY electrodes were further woven into energy devices with a maximum peak power density of 1.25 W $m^{-2}$. In addition, these devices were employed for gesture recognition and harvesting energy from water droplets.[115]

Other methods to fabricate yarn/fabric-based breathable skin-mountable electronics include nonwoven,[116] knitting,[105,117,118] embroidery,[106] and printing.[107,119,120] Here, we discuss the nonwoven technique. For instance, Sun *et al.* reported a flexible and breathable skin-mountable pressure sensor for nonwoven fabrics using MXene as an electrode and gel as an electrolyte. The fabric pressure sensor had a great sensitivity (31.4 $kPa^{-1}$) and an impressive breathability (1330.9 mm $s^{-1}$) due to its porous structure. Furthermore, it can be utilized to perform health monitoring by directly attaching to the hand and chest.[104] A dual-sided nonwoven was fabricated by electrospinning PI and vacuum filtration AgNWs. During the preparation process, the pore structure of the nonwoven was retained, which exhibited excellent breathability (65 mg $cm^{-2}$ $d^{-1}$). Additionally, the nonwoven with

Published on 03 oajagemännu 2023. Downloaded on 2026-05-06 16:33:29.

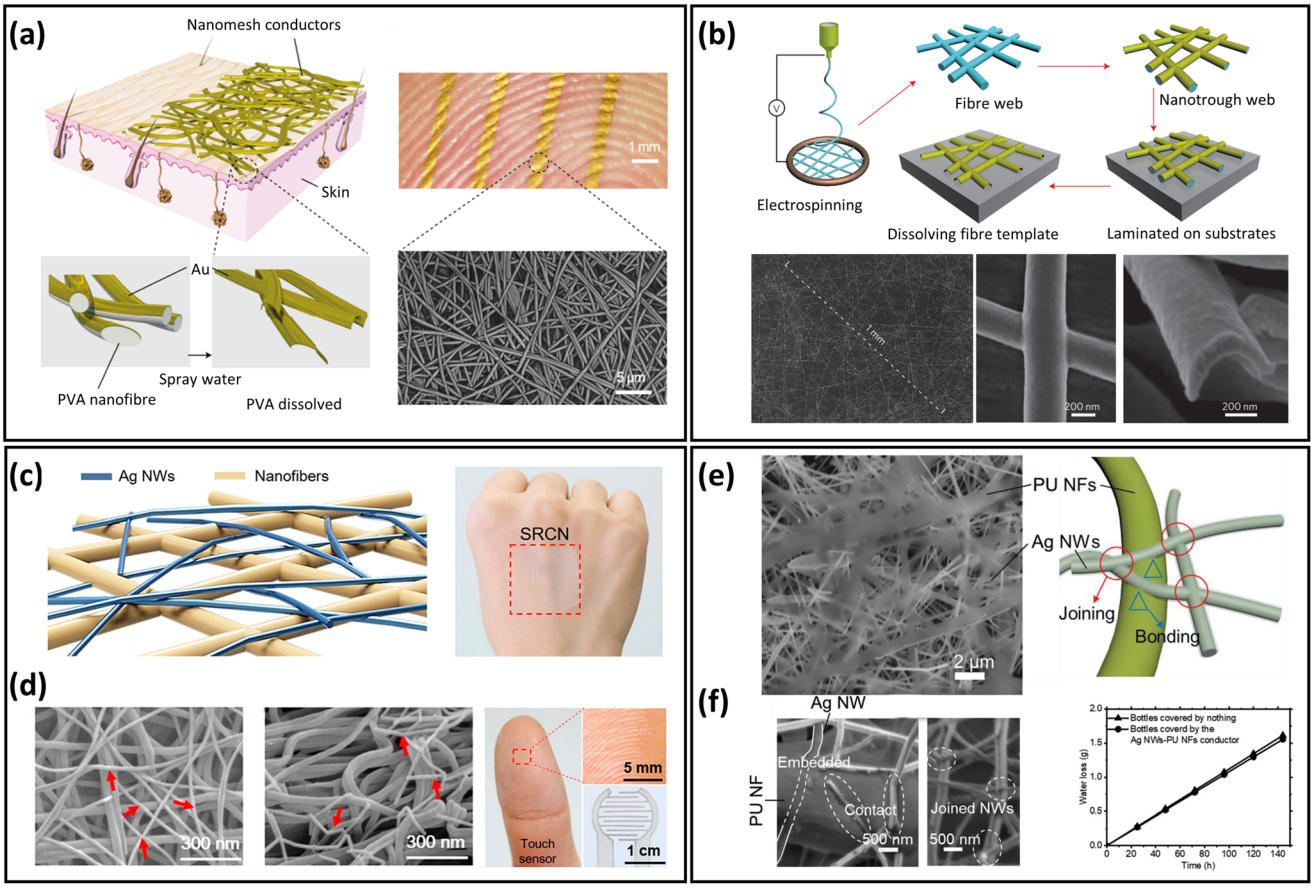


**Fig. 4** Electrospun nanofibre-based breathable skin-mountable electronics. (a) Schematic diagram of a nanomesh conductor and image of a nanomesh conductor attached to a fingertip. SEM image of a nanomesh conductor formed on a silicone skin replica by dissolving PVA nanofibers. Reproduced with permission from ref. 11. Copyright 2017 Nature Publishing Group. (b) Schematic diagram of the polymer–nanofibre template process and SEM images of its top and cross-section. Reproduced with permission from ref. 71. Copyright 2013 Nature Publishing Group. (c) Schematic diagram of the fabrication process of scaffold-reinforced conductive nanonetworks. SEM images of the scaffold-reinforced conductive nanonetworks in top-down and cross-sectional view. (d) Scaffold-enhanced conductive nanomesh attached to the back of the hand and photo of scaffold-enhanced conductive nanonetworks for touch sensors. Reproduced with permission from ref. 42. Copyright 2018 American Chemical Society. (e) SEM image of an ultra-thin porous nanomesh conductor and a schematic representation of the adhesion inside the conductor. (f) SEM image of the interface between AgNWs and PU nanofibre and gas permeability of conductor. Reproduced with permission from ref. 84. Copyright 2019 Wiley-VCH.

dense AgNWs networks possessed low electrical resistance (0.23 Ω $sq^{-1}$) and IR reflectance of over 80%. It can be employed as a personal thermal management device to achieve active electric and passive heating.[116]

In addition to physical methods, various chemical approaches have been utilized to fabricate yarn-based breathable skin-mountable electronics.[121,122] For example, Hye Moon Lee *et al.* designed a new chemical solution process (soaked $AlCl_3$ with $LiAlH_4$ in dibutyl ether $(O–(C_4H_9)_2)$ for 4 h) to deposit Al onto the fabrics to fabricate flexible electric circuits.[121] Other metals such as Ni,[122] Cu,[123] and Ag[124] can also be chemically deposited onto fabrics to make permeable skin-mountable electronics.

### 2.4 Structure design

Another typical approach to develop breathable skin-mountable electronics is structure design, primarily by fabricating porous structures to meet the permeability requirements. In this part, we will discuss representative porous devices using structure design *via* fabrication methods including templating, solution casting, breathing diagram, and hydrogel.

The template method is widely used to prepare breathable skin-mountable electronics because of its stable homogeneous size and excellent microstructure.[128,129] For instance, Min *et al.* reported a breathable conductive polymer strain sensor (Fig. 6a). It was fabricated by casting a mixture of polyurethane and conductive materials (CNTs and Ag flakes) directly onto a PDMS master mould with a hexagonal mesh pattern. The reported porous films had great stretchability (150% strain) and visible air and water permeability (Fig. 6b).[125] A limitation of the templating technique is the porous material being too thick (>5 mm), but He *et al.* reported a layered microporous composite piezoresistive sensor with a thickness of less than 1 mm. The porous PU films were prepared by the solution

 This journal is © The Royal Society of Chemistry 2023

Published on 03 oajagemánnu 2023. Downloaded on 2026-05-06 16:33:29.

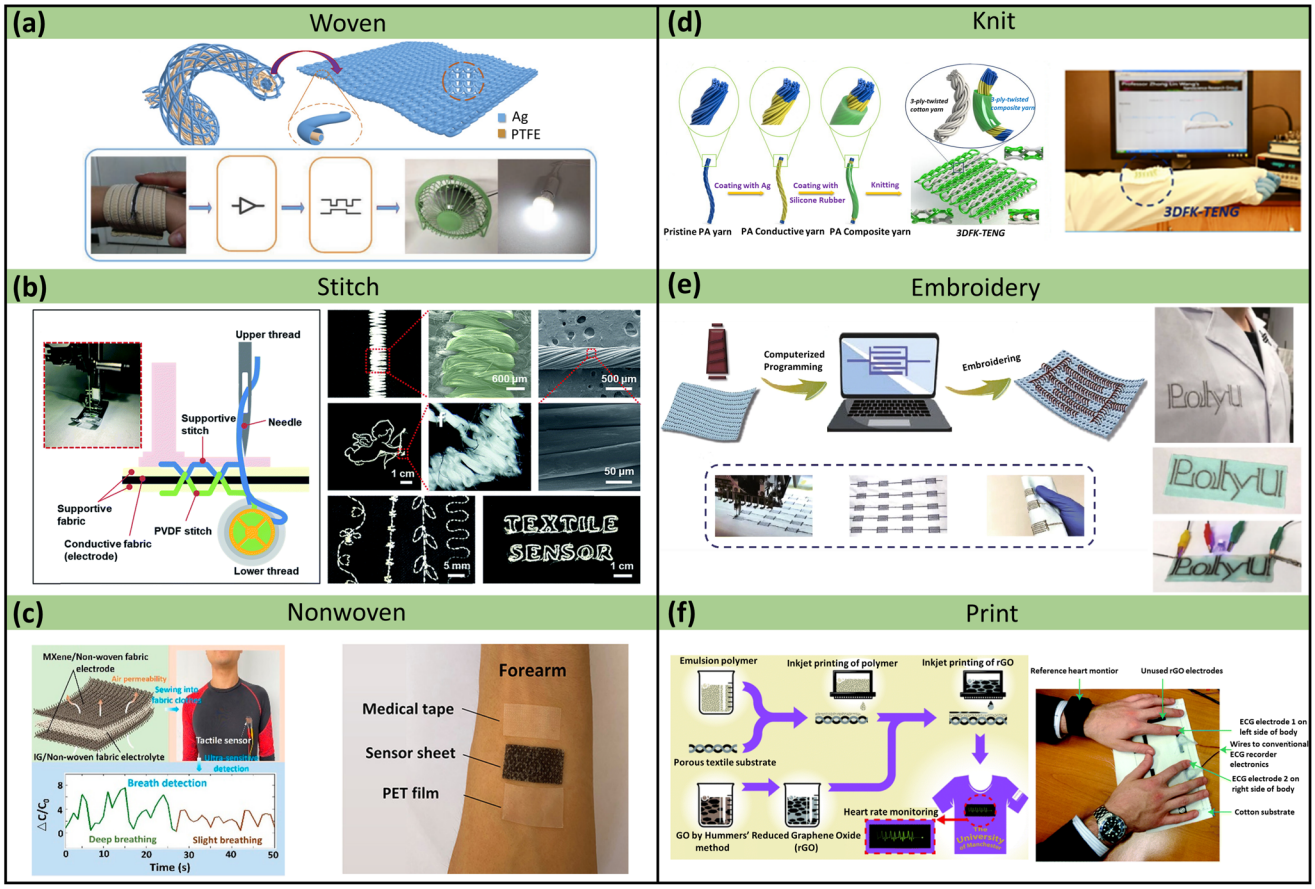


**Fig. 5** Yarn/fabric-based breathable skin-mountable electronics. (a) Schematic diagram of a coaxially structured adaptive textile and a textile in a smart home control system. Reproduced with permission from ref. 102. Copyright 2019 Wiley-VCH. (b) Schematic diagram of a textile sensor manufactured using a sewing machine and a photograph, SEM images of a PVDF stripe stitch. SEM image of the interface between AgNWs and PU NFs. Reproduced with permission from ref. 103. Copyright 2018 Royal Society of Chemistry. (c) Schematic diagram of the preparation of a fabric pressure sensor, which was successfully sewn into a tight-fitting, quick-drying garment and used to measure the respiration rate of the wearer. Schematic diagram of PET film, medical tape, and breathable sensor covering the front of the skin. Reproduced with permission from ref. 104. Copyright 2022 American Chemical Society. (d) The fabrication process of the core–sheath yarn and TENG. Reproduced with permission from ref. 105. Copyright 2020 Elsevier. (e) Schematic diagram of the preparation of conductive silver-plated nylon yarn. Reproduced with permission from ref. 106. Copyright 2019 SpringerLink. (f) Schematic diagram of the entire inkjet-printed graphene textile manufacturing process and experimental image of two fingers placed on a printed graphene patch. Reproduced with permission from ref. 107. Copyright 2017 Royal Society of Chemistry.

casting method, and were then dip-coated with CNTs (Fig. 6c). During the preparation process, the porosity of the PU film was adjusted by controlling the concentration of film solution to form porous structures with different gradients (40.27%–64.25%). The permeability of the PU@CNTs sensor was 8 times greater than that of the non-porous film, which exhibited 1802 g $m^{-2}$ $d^{-1}$ (Fig. 6d).[126] Another method is the breathing diagram, which is a simple, efficient, and scalable self-assembly process. A gas-permeable, transparent stretchable electrode was fabricated by self-assembled porous substrates and conductive nanostructures. It was composed of porous TPU nanofilms fabricated by the breath figure method and AgNWs made by dip-coating (Fig. 6e and f). The hybrid films exhibited high transmission (61%), low plate resistance (7.3 Ω $sq^{-1}$), and excellent breathability (23 mg $cm^{-2}$ $h^{-1}$). The reported permeable electrode can be employed to achieve high-quality EMG detection (24.9 dB). Furthermore, it can be used to achieve real-time response to finger touch with a response time of 0.1 s.[52]

In addition, there are a few examples of porous hydrogels for the fabrication of breathable skin-mountable electronics.[127,130] Liu *et al.* reported a flexible and adjustable porous organohydrogel, which was fabricated from gelatine/polypyrrole (PPy)/reduced graphene oxide (rGO) under mild conditions (Fig. 6g). It had a porous structure with a size of 35–650 μm due to the special fermentation process. Compared with non-penetrating polyvinyl chloride membranes, the gel/PPy/rGO organohydrogel presented excellent breathability (14 mg $cm^{-2}$ $h^{-1}$), which was superior to cotton (Fig. 6h). The porous organohydrogel was successfully employed as bioelectrical sensors to accurately monitor ECG and EMG.[127]

Published on 03 oajagemánnu 2023. Downloaded on 2026-05-06 16:33:29.

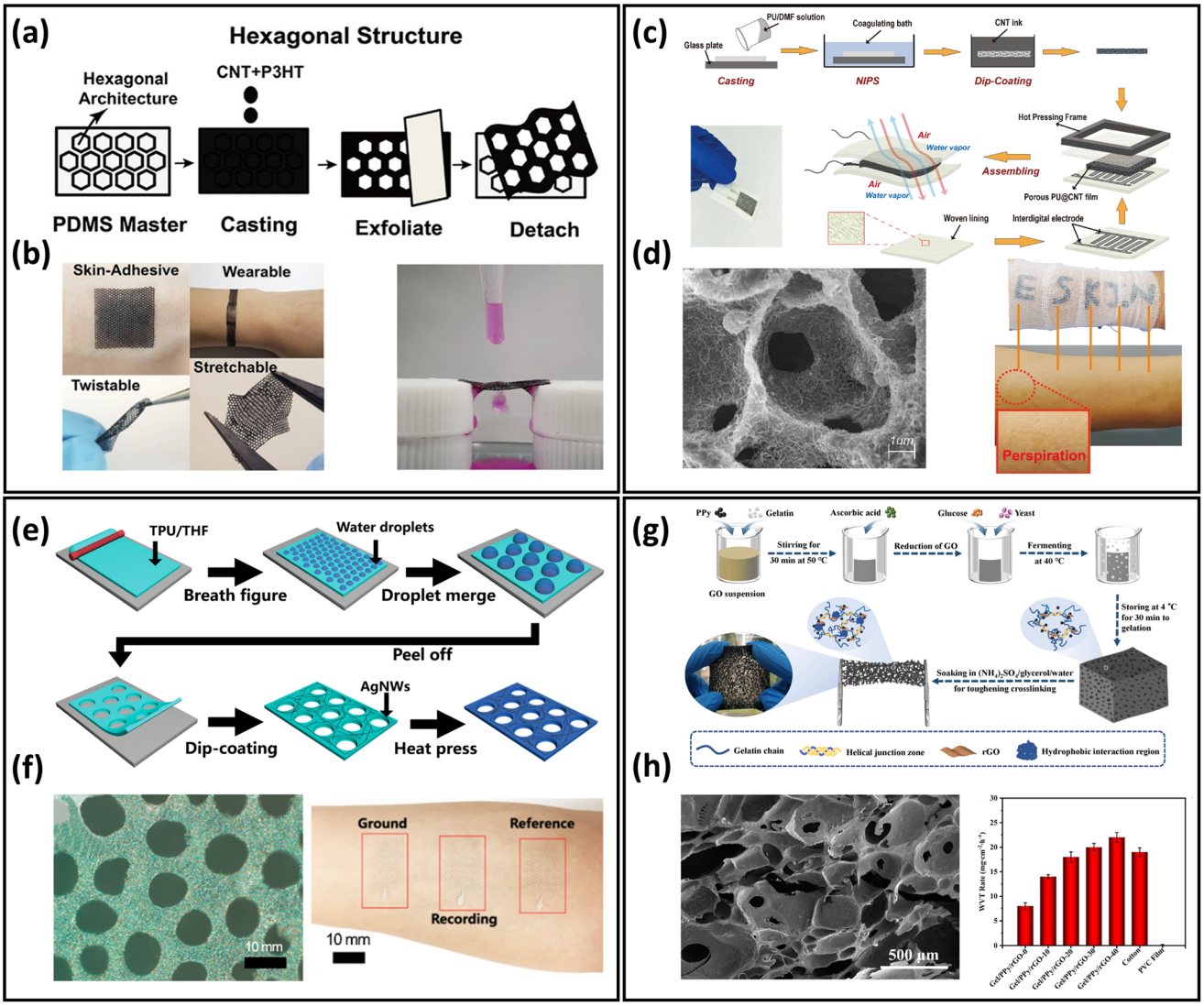


**Fig. 6** Structure design of breathable skin-mountable electronics. (a) Schematic diagram of a hexagonal lattice pattern of conductive polymer composite with a layered structure. (b) Schematic representation of the bendability, twistability, stretchability, permeability and water permeability of conductive polymer composite films. Reproduced with permission from ref. 125. Copyright 2020 American Chemical Society. (c) Schematic diagram of the preparation process of porous PU@CNT films. (d) SEM image of a cross-section of porous PU@CNT films and a schematic representation of the film attached to human skin. Reproduced with permission from ref. 126. Copyright 2020 Elsevier. (e) Schematic diagram of the fabrication process of porous AgNWs/TPU film. (f) SEM image of porous AgNWs/TPU film and photograph of an electrode attached to the forearm for EMG sensor. Reproduced with permission from ref. 52. Copyright 2022 American Chemical Society. (g) Schematic diagram of the process of fabrication gel/PPy/rGO porous organohydrogel. (h) SEM images of gel/PPy/rGO porous hydrogels and WVTR of gel/PPy/rGO porous organohydrogel, cotton, and PVC films fermented at different times. Reproduced with permission from ref. 127. Copyright 2022 Elsevier.

## 3. Properties

In on-skin applications, device functionalities and physiological comfort need to be considered for utilizing breathable skin-mountable electronics. In this section, we will discuss the following important properties: breathability, biocompatibility, adhesion, stretchability, and long-term usage.

### 3.1. Breathability

One of the principal functions of healthy human skin is to maintain the balance of heat and moisture. A person loses ~0.6–2.3 L of insensible sweat volume daily, which is equivalent to 12–42 g $m^{-2}$ $h^{-1}$.[131] If perspiration cannot quickly and sufficiently escape from the skin, moisture will accumulate on the skin surface and within the covering, leading to uncomfortable sensations such as dampness and clamminess. Poorly permeable electronics cause skin inflammation, irritation, occlusion, or other skin issues after long-term attachment. Further, the lack of breathability largely reduces the sensitivity of the monitoring signals due to sweat accumulation.[24] Here, we will introduce representative approaches to evaluate the permeability of skin-mountable electronics.


This journal is © The Royal Society of Chemistry 2023

Published on 03 oajagemännu 2023. Downloaded on 2026-05-06 16:33:29.

WVTR, the amount of water vapor passing through a film material over a period of time under a given condition (certain temperature and humidity), is considered as a typical parameter for quantifying the moisture permeability of skin-mountable electronics. ASTM E96 is commonly used as a test standard method for moisture permeability. In this method, the WVTR is usually estimated in grams per square meter per hour (or kilograms per day).[52,84] For instance, using electrospinning and printing techniques, polystyrene–butadiene–styrene (SBS)–liquid metal (LM) fibre mats were fabricated. The moisture permeability tests of the fibre mats were determined by measuring the weight loss of the water vapour in a cup with its opening firmly covered by the tested specimen at 22 °C and 63% relative humidity. During the tests, the fibre mats exhibited a superior breathability (520 g $m^{-2}$ $d^{-1}$).[132] Chen *et al.* reported an ultra-lightweight, highly permeable organic electrochemical transistor for on-skin bioelectronics. The porous fibrous electrolytes were synthesized by polymer/ionic-liquid fibres through a simple electrospinning process. To evaluate the fibres' breathability, the weight loss of water in a bottle before and after covering with fibrous membrane was measured. A negligible difference in water evaporation rate was obtained after the fibrous covering, which is the same as that under no covering, demonstrating a superior permeability (Fig. 7a and b).[133] Air permeability can be defined by ASTM D737 standard as the rate of airflow through a known area at a specific air pressure difference between two surfaces of a material, expressed in $cm^3$ $s^{-1}$ (or mm $s^{-1}$). For example, by combining electrospinning PVA and spray techniques, He *et al.* reported CNTs/PVP/PU composite thermoelectric fabrics. In this work, the YG461G automatic measuring instrument was utilized to evaluate air permeability, which exhibited an impressive result (425 mm $s^{-1}$).[134]

In addition to quantitative tests (WVTR and air flow rate), qualitative investigations can be utilized to demonstrate the breathability of skin-mountable electronics. For instance, the SBS-LM fibre mats were wrapped around a glass tube through which air was blown, demonstrating its impressive breathability (Fig. 7c). It was as permeable as human skin, enabling sweat to evaporate freely by allowing gas molecules to pass through the fibre mats.[132] Furthermore, the permeability of a fibrous PVDF-hexafluoropropylene membrane was evaluated by covering the fibre electrolytes in a beaker containing hot water. It was possible to observe small water droplets suspending on the hydrophobic surface. In addition, water vapour can pass freely through the fibre electrolytes without restrictions (Fig. 7d).[133] Besides, the permeability of the skin-mountable electronics can be demonstrated by testing skin epidermis temperature under long-term wear. For instance, a breathable PI/poly(methyl methacrylate) (PMMA)/styrene–ethylene–butylene–styrene (SEBS) film and different hybrid films were attached to the forearm of a healthy volunteer during 30 minutes of exercise. An infrared camera was utilized to measure skin temperature before and after exercise (Fig. 7e and f). Compared with different hybrid films (37.4 °C and 34.5 °C), the surface temperature of the skin covered with PI/

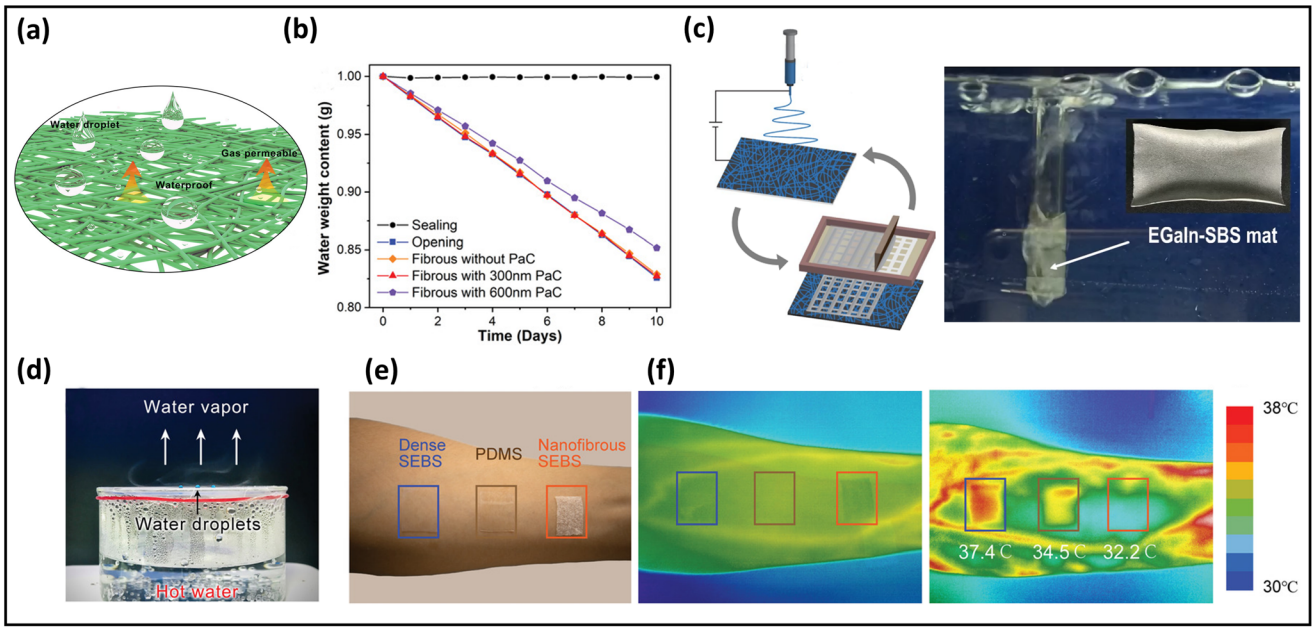


**Fig. 7** Breathability of breathable skin-mountable electronics. (a) Schematic diagram of the water droplet and permeability of fibrous electronics. (b) Different pore size is the water loss rate of the fibrous membrane. (c) Schematic illustration of the electrospun SBS fibre–EGaIn electrode and its performance in underwater permeability. Reproduced with permission from ref. 132. Copyright 2021 Nature Publishing Group. (d) Schematic diagram of water droplets suspended on a hydrophobic surface with water vapor passing freely through the fibre membrane. Reproduced with permission from ref. 133. Copyright 2022 Wiley-VCH. (e) A picture showing three different samples attached on the forearm. (f) Infrared thermal images of the skin before (middle) and after (right) running exercise. Reproduced with permission from ref. 135. Copyright 2022 Wiley-VCH.

Published on 03 oajagemánnu 2023. Downloaded on 2026-05-06 16:33:29.

PMMA/SEBS induced little variation of the skin temperature (32 °C), indicating effective cooling by sweat evaporation.[136]

### 3.2. Biocompatibility

Highly biocompatible, skin-mountable electronics can be worn for long periods without causing any allergies or rashes on human skin.[137,138] Use of biomass-based nanomaterials as the substrate of skin-mountable electronics, *e.g.*, silk protein,[139,140] gelatin,[141] cellulose,[142,143] chitin,[144] and alginate,[145] is considered as one of the most straightforward ways to achieve excellent biocompatibility for breathable skin-mountable electronics. Here, we will elaborate on silk protein. For example, Chao *et al.* reported a breathable, degradable MXene/silk protein nanocomposite-based pressure sensor. The silk protein nanofibres were prepared by electrospinning from regenerated silk films. This porous pressure sensor exhibited a wide sensing range (over 39.3 kPa), superior sensitivity (298.4 $kPa^{-1}$, 1.4–15.7 kPa), and reliable permeability (98% water retention in 25 °C, 44% humidity, 24 h). Besides, it can be employed to detect tactile signals, pressure distribution, and to recognise tiny motions, such as phonation.[146] Yan *et al.* reported a three-layer nanofibre-based epidermal electrode composed of protein nanofibres, polytetrafluoroethylene and AgNWs. The porous electrode was attached to human skin for 24 h; no redness, swelling or allergy was observed. Besides, this permeable (2553 g $m^{-2}$ $d^{-1}$ at 35 °C) electrode can successfully be utilized in ECG and EMG monitoring with high SNR (22.59 dB).[147]

*In vitro* study is considered as a representative way to quantify the biocompatibility of skin-mountable electronics.[148,149] For example, a permeable fibre mat was fabricated by coating EGaIn on electrospun SBS mats. To demonstrate the great biocompatibility of LM fibre mats, L-929 cells (as the model cell) were employed in this study. Bright-field and fluorescent live/dead staining images revealed that all samples (SBS mats, LM-SBS mats) had regular cell morphology, except for the positive control group, which had severe cell death. After 24 h, quantification of the live/dead-stained cells exhibited excellent cell viability of 95%, with no major difference between all tested groups (Fig. 8a). The absorption at 570 nm in the colorimetric assay (proportional to cell number) increased significantly with incubation time from day 1 to day 3, demonstrating that the LM fibre mats were not toxic (Fig. 8b and c). Breathable electronic devices can also improve their biocompatibility with human skin. On-skin tests were utilized to further indicate biocompatibility. Three samples were applied to the forearm of one volunteer for one week. All non-permeable samples caused significant skin erythema. In contrast, neither the SBS pad nor the EGaIn-SBS caused any negative effects on human skin (Fig. 8d).[45] It should be noted that biocompatibility and adhesion are both important properties of breathable skin-mountable electronics. Skin irritation or inflammation can be avoided due to high biocompatibility of permeable skin-mountable electronics. However, if the adhesion force of the device is too high, peeling-off will induce skin irritation after measurement. It is highly desirable to develop skin-mountable electronics with adjusted adhesion force.[150]

### 3.3. Adhesion

For breathable skin-mountable electronics, strong adhesion is essential to acquire high-quality bio-signals. For example, breathable dry electrodes with nano-scale thickness self-adhere to human skin for a long time and reduce the effects of skin deformation and sweating during signal collection. However, it has been a challenge to achieve both high permeability and strong adhesion in skin-mountable electronics.

An effective way to obtain skin adhesion is to decrease device thickness, as the mechanical conformability of a plate film is highly correlated to its flexural rigidity.[151] By reducing thickness to a few hundred nanometers, nanofilms or nanomesh structures exhibit great adhesion to human skin without external fixation methods or adhesives while maintaining great permeability.[44,152] For example, Wang *et al.* reported a self-adhesive, gas-permeable nanofilm composed of electrospun PU nanofibre and PDMS film. The nanofilms were only 95 nm thick and exhibited high area adhesion energy of 159 μJ $cm^{-2}$. These nanofilms can adhere to human skin for 1 week by van der Waals forces alone. Nanofilms behave like a "sticky" glue when being applied to and peeled off from human skin. Along with the skin's normal movements, such as stretching and contracting, the attached nanofilms can also move freely. The capacity of the nanofilm to stretch across significant lengths in all directions was attributed to the strong dynamic adhesion. Due to their excellent self-adhesion and permeability, dry electrodes made of Au-coated nanofilms were successfully employed to enable continuous monitoring of ECG signals for 1 week with a high SNR (34 dB).[49] Yang *et al.* reported an ultrathin (150 nm) epidermal electrode based on freestanding thermoplastic elastomer (TPE) nanofilms by a bubble-blowing process. It exhibited super breathability (580.18 g $m^{-2}$ $d^{-1}$), self-adhesiveness, ultrahigh sensitivity (969.3 $kPa^{-1}$), and impressive SNR (51 dB) over the wide frequency range of 0–22 000 Hz. The average peel strength of the ultrathin AgNWs-TPE electrode was 216 mN $cm^{-1}$, indicating the ability to provide secure and intimate adhesion on the target surface. In particular, the step-by-step magnified photos of the nanofilms laminated to human skin without the use of any glue exhibited great skin conformability.[153]

Besides thickness reduction, another approach is to use adhesive materials, such as silk[147,154] and hydrogel,[155,156] to develop breathable skin-mountable electronics. For instance, a skin-friendly conductive hydrogel with multiple hydrogen bonds was reported based on PVA, phytic acid (PA), and gelatin (Gel). Due to its typical porous structure, permeability (220 g $m^{-2}$ $d^{-1}$) of the PVA/PA/Gel hydrogel was guaranteed. The good adhesion of the hydrogel was attributed to the synergistic effect of hydrogen bonding and ionic bonding. The PVA/PA/Gel hydrogels were successfully attached to pigskin with a load-bearing capacity of about 100 g.[156]

To decrease the influence of sweat on device adhesion, many efforts have been made to develop breathable sweat-proof skin-mountable devices.[157,158] For instance, Rogers *et al.* reported a permeable microfluidic-based sweat sensor. The device exhibited great adhesion to the skin, even under

 This journal is © The Royal Society of Chemistry 2023

Published on 03 oajagemánnu 2023. Downloaded on 2026-05-06 16:33:29.

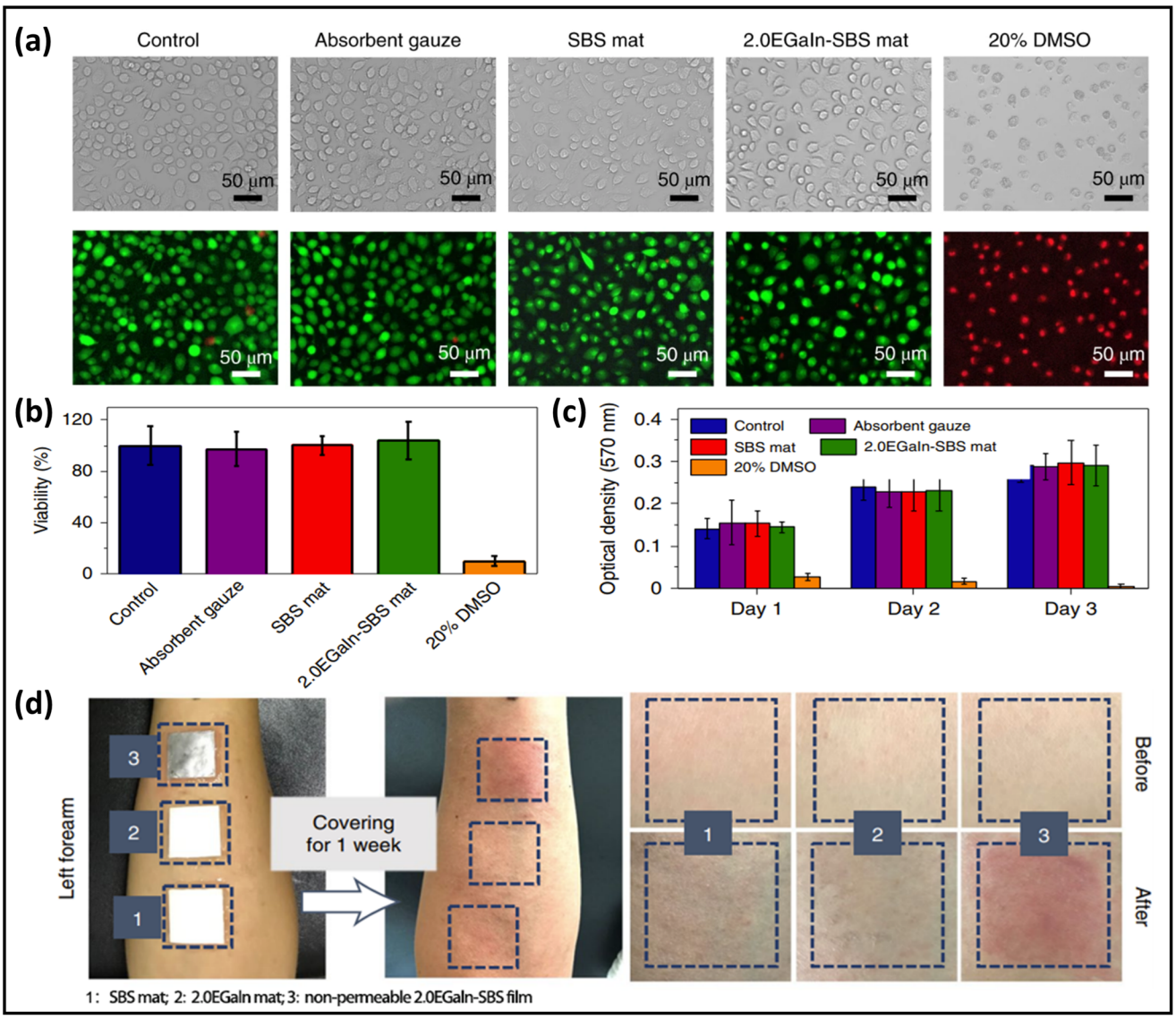


**Fig. 8** Biocompatibility of breathable skin-mountable electronics. (a) Bright field and fluorescence images of cells cultured in medium with samples. (b) Quantification of L-929 cell viability in different incubation groups. (c) Absorption at 570 nm in colorimetric assay of different incubation groups after 1, 2, and 3 days of incubation. (d) Digital images showing the results of skin irritation on the forearms of a volunteer with different materials. Reproduced with permission from ref. 132. Copyright 2021 Nature Publishing Group.

extreme sport conditions, such as 45 min swimming and 30 min biking exercise.[159] To systemically investigate the influence of sweat chemicals on adhesion performance, we need in-depth investigation in the future.

### 3.4. Stretchability

Considering that human joints can undergo a maximum deformation up to 60% strain, excellent stretchability of breathable skin-mountable electronics is emphasized. To promote conformal contact with dynamic human skin, sensors and devices that can elongate with skin deformation are required. It is worth noting that skin-mountable electronics are required to move along with large joint motions with stretchability of up to 60% strain. Furthermore, for applications in soft robots and human–machine interactive devices, breathable skin-mountable electronics require higher stretching capability of up to 1000% strain.[160,161] There are two main strategies to obtain the desired stretchability for the target applications of gas-permeable skin-mountable electronics.[38,162,163] Popular intrinsically stretchable materials include metallic/carbon-based materials, conductive polymers and stretchable elastomer substrates.[137,164] For instance, Ma *et al.* introduced LM on electrospun SEBS nanofibres to fabricate LM micromesh electrodes. They exhibited superior stretchability (>1000% strain), low surface resistance (0.38 Ω $sq^{-1}$), and great permeability (14.1 g $m^{-2}$ $h^{-1}$). In optical images, LM micromesh had uniform colour distributions even when stretched to 1000% strain. It provided sufficient internal space for the microfibres due to the porous structure. The actual strain on the individual microfibres was mostly mitigated by bending deformation. In addition, the prepared LM micromesh

Published on 03 oajagemánnu 2023. Downloaded on 2026-05-06 16:33:29.

electrodes can be attached to human skin for 12 h continuously without any adverse reactions. These electrodes were successfully utilized for EMG monitoring with a high SNR (23 dB).[165]

The other strategy is to design breathable conductors or devices with extrinsic structures. For example, corrugated structures, and kirigami structures were employed to achieve the stretchability of breathable skin-mountable electronics.[166–168] Here, we elaborate kirigami structures. Li *et al.* reported a kirigami-structured electrode using an electrospinning SEBS and laser cutting technique. The device exhibited an ultralow modulus of 5 kPa in 50% strain, which was attributed to the kirigami structure. The WVTR of a continuous SEBS nanofibrous structure with no kirigami was eight times higher than that of a 100 μm-thick PDMS film.[136] Xu *et al.* developed a breathable kirigami-shaped ionotronic strain sensor by integrating silk fabric and ionic hydrogel. The fabricated sensor exhibited excellent breathability (542.3 mm $s^{-1}$) due to the porous loop structure. It can be stretched up to 100% strain and showed great mechanical stability (over 1000 cycles at 20% strain).[169]

### 3.5. Long-term usage

Long-term usage of breathable skin-mountable electronics is very significant, especially in vital sign monitoring for individualized health care management. It requires a deep understanding of the relationship between porous material structure and device performance.[170,171] Among the existing breathable skin-mountable electronics, certain achievements for long-term usage have been reported.[172–174] Creating a robust device/skin interface is the main method to fabricate breathable skin-mountable electronics for long-term use.[175]

A fully perforated skin-mountable device inspired by sweat pores was developed by Yeon *et al.* By fabricating PI films and porous PDMS binders to form an engineered pore pattern (dumbbell holes), the sweat pathways and stable mechanical properties of the sensor are guaranteed. The transepidermal water loss rate was measured to evaluate the vapor permeability of the sensor (94.54% transepidermal water loss). Sodium lauryl sulfate solution was used to induce erythema on the skin. The recovery of the damaged skin was tested in three stages by using a corneometer. The skin area laminated by this sensor exhibited the exact same track of skin recovery over 2 weeks as measured by the corneometer. Furthermore, the hydration sensor was successfully employed for long-term health monitoring, including skin regeneration tracks and daily activity checks over a 1-week period.[176]

Nanofibres with porous structure are popular materials for the preparation of breathable skin-mountable electronics to achieve long-term usage.[25] For instance, Nayeem *et al.* reported an all-fibre-based mechanoacoustic sensor composed of electrospun PVDF/PU nanofibres. Owing to the porous structure of nanofibre layers, the sensor indicated excellent breathability (12.4 kg $m^{-2}$ $d^{-1}$). In addition, with the sensors attached to the human chest the stable monitoring of heart rate was performed over 10 h with high SNR (40.9 dB).[179] Recently, Wang *et al.* reported an ultrathin, breathable PU/PDMS nanofilm with a thickness of only 95 nm. The nanofilm exhibited great area skin adhesion energy (159 μJ $cm^{-2}$). The assembled Au/PU/PDMS dry electrodes can self-adhere to human skin by van der Waals forces and have a high SNR (34 dB) with continuous ECG monitoring for 1 week.[49]

## 4. Soft electronic applications

In this section, we will discuss recent representative applications of breathable skin-mountable electronics, such as bioelectrical sensors, temperature sensors, humidity and hydration sensors, strain and pressure sensors, energy harvesting and storage devices, *etc*.

### 4.1. Bioelectrical sensors

Breathable skin-mountable bioelectrical sensors can measure biopotential signals through the skin non-invasively. They can be classified as gel-assisted wet electrodes and dry electrodes.[180] Typical bioelectrical signals include ECG, EEG, EMG and EOG. In this part, we will discuss gas-permeable skin-mountable dry electrodes.

Efforts are underway to develop gas-permeable skin-mountable bioelectrical sensors.[181–185] One method is to fabricate electronic tattoos.[25,186] For example, a breathable electronic tattoo sensor was prepared using laser-induced hierarchical carbon nanofibres (LIHCNFs). The dehydrofluorinated CNTs were firstly attached to porous PDMS substrates by a double-sided biomedical tape, then an electronic tattoo with a spider web shape was fabricated by direct laser scribing and cutting instructions (Fig. 9a). The bioelectrical tattoo had a great permeability (14 mg $cm^{-2}$ $h^{-1}$) due to its porous substrate, and can be utilized for ECG, EMG and EEG monitoring.[177] ECG signals can be derived by directly measuring the distance from the LIHCNF tattoos to the vibrator (Fig. 9b). The LIHCNFs tattoo had a low impedance (23.59 kΩ $cm^2$). It can be utilized to distinguish the low-strength EMG signals generated by the fingers executing bending or extension (Fig. 9c). The electronic tattoo can be used to identify EMG signals in different finger movements (H, E, L, L, and O). EEG signals can be detected at low frequencies (8–13 Hz) by attaching the electronic tattoo to the volunteer's forehead (eyes closed and opened) (Fig. 9d).[177]

The other method is to fabricate bioelectrical sensors based on porous substrates. Various conductive materials, such as metals, carbon-based materials, and conductive polymers, can be grown *in situ* on porous substrates. Graphene, CNTs, and their composite as porous substrates can be produced by chemical reduction and laser-induced graphitization.[188,189] For example, Xu *et al.* reported an ultrathin (90 μm), permeable PU-graphene EOG sensor. It was firstly prepared using laser-induced honeycomb graphene, then transferred onto a piece of PU tape (Fig. 9e and f). The thickness of the honeycomb graphene was about 100 nm, as shown in SEM images. Such porous structures ensured the great breathability of graphene electrodes. These electrodes were attached to eyes for EOG monitoring. Two electrodes (named C and D) were placed above the eyebrow and below the eye, and showed that the eye-

 This journal is © The Royal Society of Chemistry 2023

Published on 03 oajagemánnu 2023. Downloaded on 2026-05-06 16:33:29.

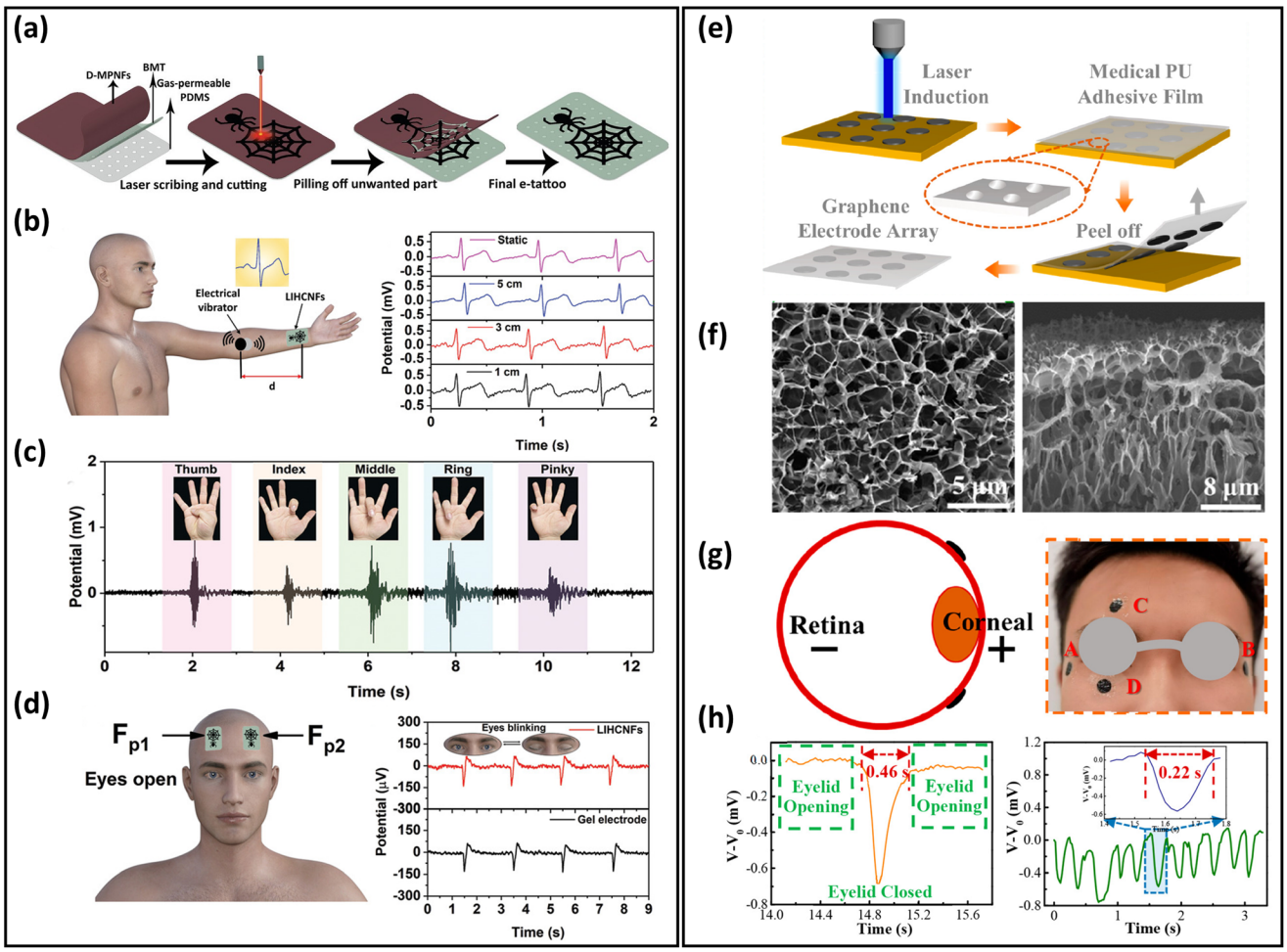


**Fig. 9** Breathable skin-mountable bioelectrical sensors. (a) Schematic illustration of the fabrication of electronic tattoos based on LIHCNFs. (b) Schematic diagram of the ECG test and ECG signals at different measurement distances. (c) EMG signals generated by different gestures. (d) Position of the electronic tattoo in the eye in EEG testing and EEG signal values of electronic tattoos and commercial electrodes. Reproduced with permission from ref. 177. Copyright 2021 Wiley-VCH. (e) Fabrication procedure of breathable honeycomb graphene electrode arrays. (f) SEM images of the graphene electrode surface and cross-section. (g) Schematic diagram of graphene electrodes attached around the human eye during EEG testing. (h) Single-cycle blink signals and continuous fast eye-blink signals extracted from part D. Reproduced with permission from ref. 178. Copyright 2022 American Chemical Society.

blink period was 1.15 s. The period between opening and closing the eyes of the volunteers was 0.46 s, and the amplitude of the output signal was approximately −0.68 mV with excellent SNR (38.7 dB) (Fig. 9g and h).[178]

### 4.2. Temperature sensors

Accurate, real-time detection of body temperature changes is critical for thermal homeostasis analysis and understanding complex health conditions in the human body. It is noteworthy that deviation of a few degrees from core body temperature can cause impairment or even death. Immense efforts have been dedicated to developing breathable skin-mountable temperature sensors.[190–192]

Typical breathable skin-mountable temperature sensors are thermo-sensitive conductive composites and conductors. Nanofibres/fabrics have been used as porous substrates for the fabrication of breathable skin-mountable temperature sensors. These porous-structured temperature sensors were attractive alternatives to perform versatile functions in continuous healthcare monitoring systems.[208,209] For example, based on electrospun Pt nanofibres, AgNWs nanofibres and silk fibroin, an integrated thermo-sensitive temperature sensor had great sensitivity (0.205% $°C^{-1}$) and excellent air permeability (21.2 mm $s^{-1}$). Notably, a stable cycle of resistance changes responding to temperature ranges from 20 °C and 60 °C was maintained over 70 000 s, indicating the high reliability of this temperature sensor. Pt nanofibre temperature sensor cells were stuck onto fingers that grasped a hot water cup. The temperature values converted by the change in resistance of the Pt nanofibers sensors exhibited small variation (<0.5 °C) compared with the temperature detected by commercial thermometers. In addition, an integrated device facilitated personal thermal management for arthritis relief in physiotherapy.[193] Chen *et al.* reported a TPU/ionic liquid fibrous mat

Published on 03 oajagemännu 2023. Downloaded on 2026-05-06 16:33:29.

developed through solution blending and electrospinning. Owing to the porous structures, the gas from an injector could easily pass through the nanofibre ionogel mats into the water. This demonstrated that the nanofibre ionogel mats had impressive breathability (532.45 g $m^{-2}$ $d^{-1}$). The mats were then assembled into a breathable temperature sensor. Due to the accelerated ion mobility with increasing temperature, the temperature resistance change value decreased monotonically as the temperature increased from 30 °C to 100 °C. This fibre mat temperature sensor showed a superior thermal sensitivity (2.75% $°C^{-1}$), which was superior to the traditional temperature sensor. The accuracy of the sensor in temperature monitoring was evaluated by investigating the resistance response of the sensor to a step increase in temperature from 37 °C to 38 °C in 0.1 °C intervals. In addition, the response time of the temperature sensor was 2.46 s, which was much shorter than that of a commercial mercurial thermometer.[90] To improve the stability of breathable temperature sensors under harsh conditions, Luo *et al.* developed a superhydrophobic and breathable textile-based sensor. Firstly, dopamine was used to modify the original elastic textile. MXene nanosheets with a large number of functional groups were coated onto the fibre surface by dip coating. Lastly, a PDMS layer was used to package the dopamine/MXene textiles. The as-fabricated temperature sensor exhibited great breathability and excellent waterproof performance. With an excellent photoelectro-thermal response, the breathable temperature sensor showed a wide temperature-measuring range (25–100 °C) and a high temperature coefficient resistance (−1.8% $°C^{-1}$).[204]

In addition, ultra-sensitive skin-temperature sensors are important for developing breathable skin-mountable electronics.[205–207] For instance, Jaeho Shin *et al.* reported a highly flexible NiO temperature sensor. It was designed by using a combined strategy of monolithic and low thermal budget laser activation processes, and exhibited an excellent sensitivity (−9.2% $°C^{-1}$) and a high level of integrity.[207] Table 1 provides a summary of breathable skin-mountable temperature sensors in the last five years.

### 4.3. Humidity and hydration sensors

Humidity and hydration sensors have been extensively developed over the past two decades, and have been employed in various wearable applications such as breathing behaviour, noncontact switch, and baby diaper monitoring.[27,210,211] Many researchers have been working to improve the performance of breathable skin-mountable humidity and hydration sensors.[212–214] Here, we will discuss the breathable skin-mountable humidity and hydration sensors separately.

A typical example is the gas-permeable nanomesh humidity sensor. In brief, by deposition of Parylene C and Au, a humidity sensor was assembled onto electrospun PVA nanomesh (Fig. 10a and b). By attaching a humidity sensor to human skin, the impedance changes under different body states were tested through artificially adjusting the skin humidity (Fig. 10c). The humidity sensor was also attached to the surface of a human back that released sweat through exercise (30 push-ups) to increase skin humidity. The results show that the humidity sensor resistance's real-time changes can be displayed (Fig. 10d) at a constant ambient humidity (25%).[187] In addition, hybrid nanofilms can be utilized to prepare breathable skin-mountable humidity sensors.[215–217] For instance, a breathable humidity sensor composed of cellulose nanocrystal/iron(III) ion/PVA (CNC/$Fe^{3+}$/PVA) hybrid film was fabricated. Due to the porous structure of the CNC/$Fe^{3+}$/PVA film, the sensor showed excellent permeability (3.03 kg $m^{-2}$ $d^{-1}$). When the hybrid film mounted on skin was connected to a multimeter, the real-time change of temperature and humidity of the skin could be monitored.[218] Yue *et al.* reported a collagen

**Table 1** Summary of breathable skin-mountable temperature sensors in the last five years

| Materials | Breathability | Sensitivity | Temperature range | Ref. |
|---|---|---|---|---|
| Pt networks/silk fibroin composite membranes | — | 0.205% $°C^{-1}$ | — | 193 |
| MOX/C-PNHM | 90% water remaining after 7 days | 0.23% $°C^{-1}$ | 30–70 °C | 191 |
| Ionic liquid/TPU | 427.62–532.45 g $m^{-2}$ $d^{-1}$ | 3.28% $°C^{-1}$ | 30–100 °C | 90 |
| Graphene/Cellulose | Soaked in 5% paraformaldehyde in 24 h | −0.195% $°C^{-1}$ | 30–50 °C | 194 |
| AgNWs/TPU/PET | 7.1 mg $h^{-1}$ | 0.88% $°C^{-1}$ | 28–45 °C | 195 |
| SEBS/PMMA | 1.6 g $m^{-2}$ $h^{-1}$ | — | 10–30 °C | 196 |
| AgNWs/PI | — | 0.47 Ω $°C^{-1}$ | 25–60 °C | 197 |
| MCNT/PDMS | — | — | 10–60 °C | 198 |
| Graphene fibre/Lycra warp | 48 g $m^{-2}$ $h^{-1}$ | — | 20–40 °C | 88 |
| PVA/PVDF | 20% air permeation | 0.0075 Ω $°C^{-1}$ | 25–55 °C | 199 |
| SEBS/AgNWs | 0.0206 g $cm^{-2}$ $h^{-1}$ | $2.14 \times 10^{-3°}$ $C^{-1}$ | 20–60 °C | 200 |
| PEDOT:PSS/spacer fabric | 102.85 mm $s^{-1}$ | 25 μV $K^{-1}$ | 10–60 K | 201 |
| PCB/PI | 31.04% air permeation | — | 25–40 °C | 202 |
| CNC/$Fe^{3+}$/PVA | 3.03 kg $m^{-2}$ $d^{-1}$ | 4.29% $°C^{-1}$ | 25–175 °C | 203 |
| PDA/MXene/PDMS | 0.55 kg $m^{-2}$ $h^{-1}$ | −1.8% $°C^{-1}$ | 25–100 °C | 204 |
| Ag/AAm/AAc | — | −0.0289% $°C^{-1}$ | 27–40 °C | 205 |
| Au/SiNM | — | −37 270.72 ppm $°C^{-1}$ | 25–40 °C | 206 |
| PET/NiO | — | −9.2% $°C^{-1}$ | 25–70 °C | 207 |

MOX moxifloxacin hydrochloride, C-PNHM thermoresponsive poly(*N*-isopropyl acrylamide-co*N*-methylol acrylamide), PI polyimide, PCB printed circuit board, PDA polydopamine, SiNM silicon nanomembrane, PET poly(ethylene terephthalate), AAm acrylamide, AAC acrylic acid.

 This journal is © The Royal Society of Chemistry 2023

Published on 03 oajagemánnu 2023. Downloaded on 2026-05-06 16:33:29.

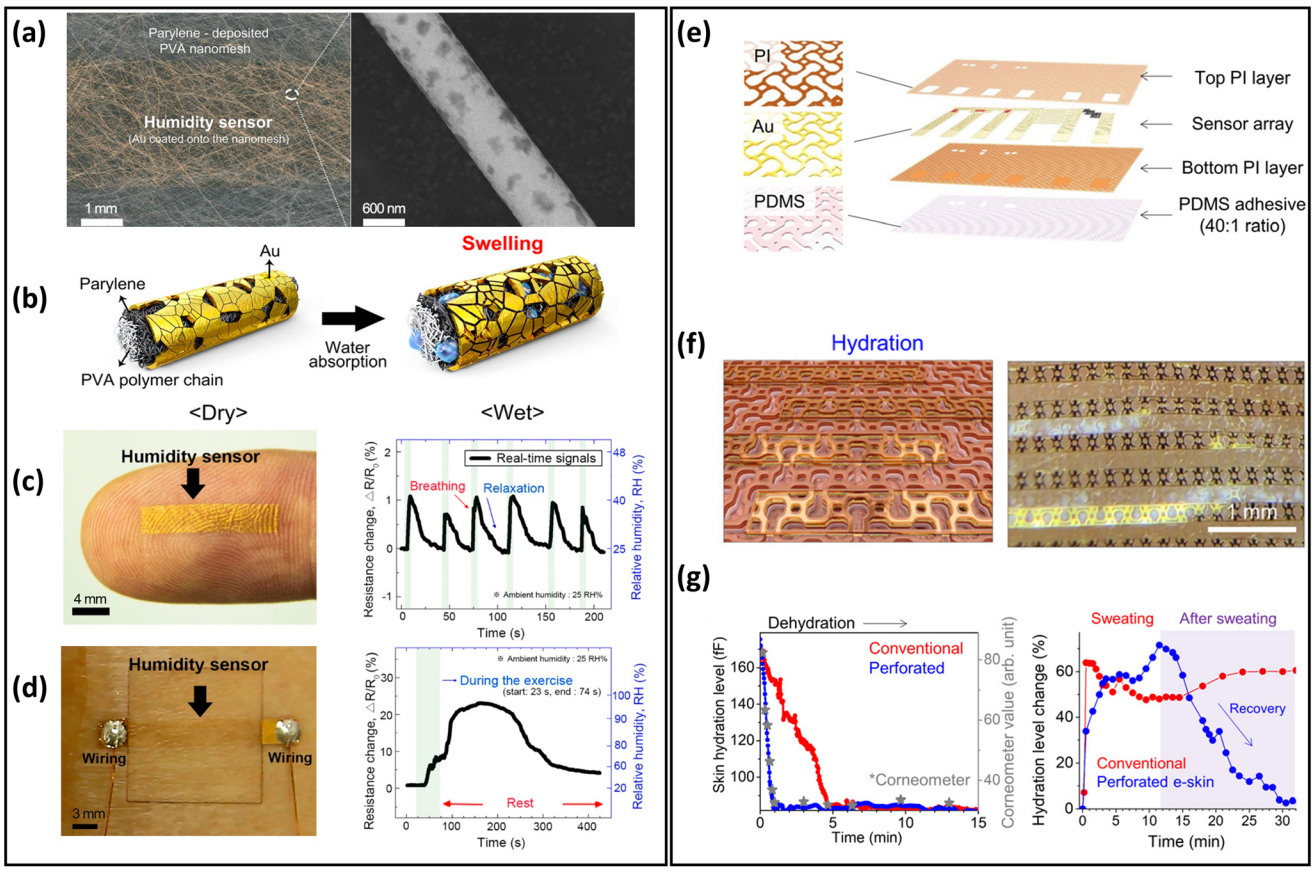


**Fig. 10** Breathable skin-mountable humidity and hydration sensors. (a) Schematic diagram of nanomesh humidity sensor and SEM image of the single nanofiber. (b) Schematic diagram of the working principle of the humidity sensor. (c) Humidity sensor images of human fingers and real-time sensor response to human breath. (d) Image of the humidity sensor on the back of the body and the real-time response of the sensor to sweat. Reproduced with permission from ref. 187. Copyright 2019 American Chemical Society. (e) Schematic diagram of perforated sensor with auxiliary dumbbell through-hole pattern. (f) Schematic diagram of capacitive-type gold hydration sensor. (g) Dehydration monitoring of the moisturized forearm and curve of changes in skin hydration levels after heavy forehead sweating. Reproduced with permission from ref. 171. Copyright 2021 American Association for the Advancement of Science.

aggregate/bead-chain-net PVA/PVDF hybrid nanofilm by electrospinning. The hybrid film-assembled humidity sensor exhibited great air permeability (20.87 mm $s^{-1}$), rapid response time (16 s), and fast recovery time (25 s) under a wide humidity range (25–85%).[199]

Skin hydration is a significant indicator of human physiology. Particularly during prolonged exercise, abnormalities in hydration will cause serious health problems, *e.g.*, headache, tiredness and dry mouth.[25,219] To achieve breathable skin-mountable hydration sensors, the main strategy is to prepare sensors based on porous substrates.[217,220] Inspired by human sweat pores, Yeon *et al.* reported a skin hydration sensor with a perforated dumbbell-shaped structure. The auxetic dumbbell hole patterns were integrated into the modules to fabricate the skin electronics, including the electronic components (Au interconnects and PI packages) as well as the PDMS adhesive (Fig. 10e and f). The porous hydration sensor exhibited excellent permeability (94.54% ± 7.33% trans-epidermal water loss). The quantitative analysis of the sweat retention area was measured by an image analyser. The results proved that sweat was effectively drained from the perforated skin electronics. The hydration level of the forearm was qualified by this sensor, which showed a level consistent with that of commercial sensors after 15 min continuous testing (Fig. 10g).[171]

### 4.4. Strain and pressure sensors

Over the last two decades, significant advancements in strain and pressure sensors have been obtained in a variety of applications in robotics, prosthetics, wearables, and health monitoring because of their extensive customizability, convenience of integration, and outstanding mechanical performance.[221–224] Nanofibres as porous substrates have been applied to prepare breathable strain sensors due to their excellent permeability and superior mechanical properties.[84,101,153,170] For example, a novel breathable skin-mountable strain sensor was fabricated by electrospinning TPU fibres on a polyethylene terephthalate support, and then AgNWs solution was sprayed onto the fibres. A finely optimized photonic sintering process was introduced to increase the durability (10 000 cycles at 40% strain) of the AgNWs/TPU sensor. Besides, the strain sensor

Published on 03 oajagemännu 2023. Downloaded on 2026-05-06 16:33:29.

showed excellent breathability (7.1 mg $h^{-1}$) due to its porous structures.[195] Conductive inks can be applied to TPU fibres to fabricate strain sensors as well. The sensors achieved great air permeability (80 mm $s^{-1}$), impressive stretchability (GF = 520), and a wide operating range (up to 500% strain).[225] Wang *et al.* reported a breathable strain sensor based on carbonized silk fabrics. The original silk fabric was carbonized by heat treatment under an inert atmosphere and then further encapsulated (Fig. 11a). The warp yarn of this structure was composed of twisted silk fibres and the weft yarn was consisted of parallel silk fibres. The strain sensor made from such a structure showed high sensitivity, with strains of up to 520% strain and fast response time (70 ms) (Fig. 11b). Due to the excellent flexibility and high sensitivity, this sensor can be used in wearable devices to monitor human activity in real time, *e.g.*, voice monitoring and knee movement monitoring (Fig. 11c).[226] Table 2 summarizes representative breathable skin-mountable strain sensors in the last five years.

Gas-permeable skin-mountable pressure sensors have been used to evaluate external stimuli on curvilinear and dynamic human skin surfaces.[228] A typical approach is to use fibres as conductive/dielectric layers (one or more layers) to assemble breathable skin-mountable pressure sensors.[28,229] Based on pressure-sensing mechanisms, there are four different types: piezoresistive, capacitive, piezoelectric, and triboelectric.[230,231] Fu *et al.* reported a sandwich-structured gas-permeable capacitive pressure sensor, which was composed of electrospun $TiO_2$ nanofibres, AgNWs, and PI films (Fig. 11d). The capacitive pressure sensor was highly breathable. The water evaporation rate of the sensor exhibited a rapid deceased of the water content by 57.6% at 65 °C for 48 h, which was attributed to the porosity of the $TiO_2$ nanofibre network (Fig. 11e). Owing to the excellent mechanical stability of the ceramic nanofibre network, the pressure sensor exhibited superior durability (50 000 cycles at 1 kPa). Also, it achieved real-time health monitoring (Fig. 11f).[227]

Breathable skin-mountable devices based on other pressure-sensing mechanisms (piezoresistive, triboelectric, and piezoelectric) have also been reported.[232–234] For instance, Zheng *et al.* developed a MXene/CNTs/cellulose nanofibre piezoresistive pressure sensor through a layer-by-layer assem-

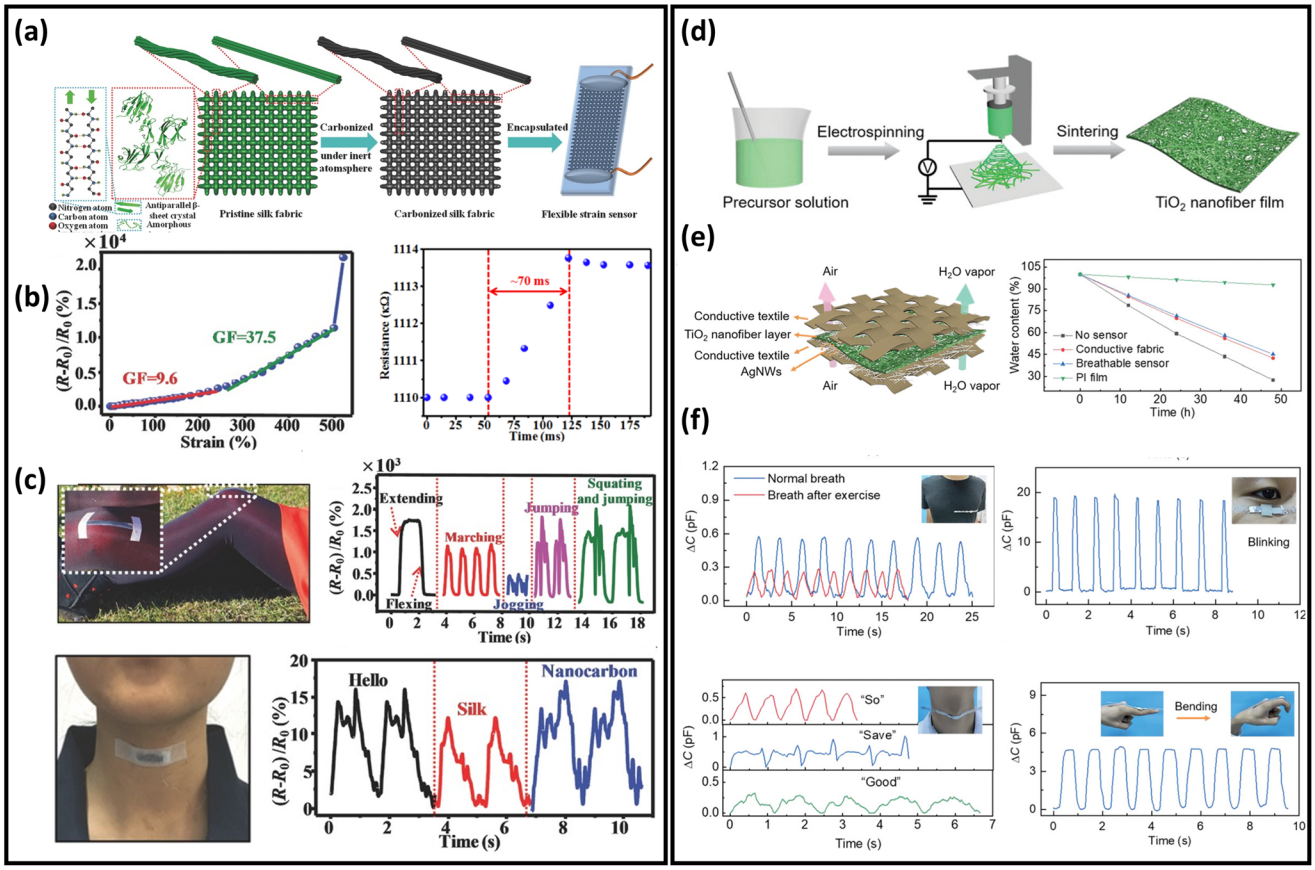


**Fig. 11** Breathable skin-mountable strain and pressure sensors. (a) Schematic representation of the layered structure and manufacture of the carbonized silk fabrics strain sensor. (b) Relative change in resistance *versus* strain curve and response curve for the carbonized silk fabrics strain sensor. (c) Silk fabric-derived hierarchically structured carbon-based flexible strain sensors for speech monitoring and knee-joint-motion monitoring. Reproduced with permission from ref. 226. Copyright 2016 Wiley-VCH. (d) Schematic diagram of the fabrication process of the $TiO_2$ nanofibre network. (e) Schematic diagram of a breathable and wearable sensor and water evaporation experiment. (f) Breathable pressure sensors for real-time and *in situ* human physiological monitoring (breathing monitoring before and after exercise, blink monitoring, sound monitoring, and finger flexion monitoring). Reproduced with permission from ref. 227. Copyright 2020 Wiley-VCH.


This journal is © The Royal Society of Chemistry 2023

Published on 03 oajagemánnu 2023. Downloaded on 2026-05-06 16:33:29.

Table 2 Summary of breathable skin-mountable strain sensors in the last five years

| Materials | Breathability | GF | Stretchability | Durability | Ref. |
|---|---|---|---|---|---|
| Copper/PVA | 25 g $m^{-2}$ $h^{-1}$ | 49.5 | 100% | 3000 cycles (50% strain) | 101 |
| PDMS/CNT/CB | 10.9375 mg $cm^{-2}$ $h^{-1}$ | 7.747 | 80% | 10 000 cycles (30%) | 237 |
| PDA/MXene/PDMS | 0.55 kg $m^{-2}$ $h^{-1}$ | 0.68–3.50 | 100% | 100 cycles (20% strain) | 204 |
| Graphene fibre/Lycra warp | 48 g $m^{-2}$ $h^{-1}$ | 63 | 48.5% | 3000 cycles (30% strain) | 88 |
| Ionic liquid/TPU | 427.62–532.45 g $m^{-2}$ $d^{-1}$ | — | 200% | 1000 cycles (100% strain) | 90 |
| MXene/nylon | — | 24.35 | 20% | 500 cycles (6% strain) | 238 |
| Conductive polyester fabric/Al-doped ZnO | 33.2 g $m^{-2}$ $h^{-1}$ | (−2.12)–(−0.06) | 130% | 3000 cycles (20% strain) | 239 |
| Single-walled CNTs/Cotton bandage | 1200 g $m^{-2}$ $d^{-1}$ | 1.2–6 | 150% | 50 000 cycles (40% strain) | 240 |
| AgNWs/TPU/PET | 7.1 mg $h^{-1}$ | 30–125 | 50% | 10 000 cycles (40% strain) | 195 |
| CNC/$Fe^{3+}$/PVA | 3.03 kg $m^{-2}$ $d^{-1}$ | 7.64 | 80% | 5000 cycles (40%) | 203 |
| rGO/Spandex fabric/PDMS | 13.6 mg $cm^{-2}$ $h^{-1}$ | 17.7 | 70% | 14 500 cycles (30% strain) | 241 |
| CNTs/PU/PVA | 400 mm $s^{-1}$ | 2.5 | 250% | — | 134 |
| TPU/polyester | 80 mm $s^{-1}$ | 520 | 500% | 1000 cycles (30% strain) | 225 |
| CB/TPU/CNTs/F-$SiO_2$ | 125 mm $s^{-1}$ | 12.05–60.42 | 100% | 1000 cycles (70% strain) | 242 |
| Graphene nanoribbons/TPU | — | 35.7 | 100% | 5000 cycles (100% strain) | 243 |
| AgNWs/TPE | 580.18 g $m^{-2}$ $d^{-1}$ | — | 62% | — | 153 |
| AgNWs/PU | 9.9 mg $cm^{-2}$ $h^{-1}$ | — | 310% | 1000 cycles (82% strain) | 84 |
| α-CD/C9-PVA/glycerol | 726 g $m^{-2}$ $d^{-1}$ | — | 598% | 1500 cycles (20% strain) | 244 |
| $MoS_2$/isopropanol/Au film | 4.4 mg $cm^{-2}$ $h^{-1}$ | — | 100% | 100 cycles (40% strain) | 245 |
| EO/AMS /Polyacrylate | — | 0.7524–1.9428 | 100% | 400 cycles (20% strain) | 246 |
| Carbonized silk fabric/PDMS | — | 9.6–37.5 | 500% | 6000 cycles (100% strain) | 226 |
| Silk fabric/AAm/LiCl/APS/MBAA | 542 mm $s^{-1}$ | — | 100% | 10 000 cycles (10% strain) | 169 |

CB carbon black, α-CD α-cyclodextrin, EO essential oil, AMS load mesoporous silica, AAm acrylamide, APS ammonium persulfate, MBAA *N,N*-methylenebisacrylamide.

bly and roll-to-roll process. The sensor had excellent air permeability (838.7 ± 22.6 mm $s^{-1}$) due to its porous structure. Also, a bark-shaped CNT/MXene-decorated pressure sensor had a high sensitivity (0.245 $kPa^{-1}$) and a wide response range (0.128–12.9 kPa).[235] Li *et al.* reported a triboelectric pressure sensor composed of all-fibre structures (hydrophobic PVDF nanofibres, conductive carbon nanofibres, and PU nanofibres). This pressure sensor exhibited an impressive permeability (10.26 kg $m^{-2}$ $d^{-1}$) and a high sensitivity (0.18 V $kPa^{-1}$) over a range of 0–175 kPa.[236] To optimize piezoelectric responses, a breathable pressure sensor was fabricated by electrospinning PU, PVDF-trifluoroethylene/$BaTiO_3$ and CNTs. The all-fibre based structures determined the great air permeability (565.43 g $m^{-2}$ $d^{-1}$) of the pressure sensor. In addition, the sensor was repeatedly loaded/unloaded over 12 000 cycles at a constant force of 5 N, and the current output performance remained almost unchanged, demonstrating excellent stability.[232] Table 3 summarizes breathable skin-mountable pressure sensors in the last five years.

### 4.5. Energy-harvesting devices

Energy-harvesting devices collect energy from the environment (solar, thermal, mechanical, *etc.*) and convert it into electrical energy. They are capable of providing sustainable power, realizing long-term usage of breathable skin-mountable electronics.[257,258] For instance, self-powered sensors, *i.e.*, human motion sensors, can convert small-scale energy from vibrations and motions into electrical power. Furthermore, such energy can be utilized for real-time health monitoring.

Porous materials such as electrospun nanofibres,[259,260] fabrics,[261–263] and paper[264] have been widely used to fabricate typical breathable skin-mountable harvesting devices, *e.g.*, TENG[265–267] and piezoelectric nanogenerators (PENG).[268,269] For example, Shi *et al.* developed a gas-permeable skin-mountable TENG, which was composed of electrospun TPU nanofibres, AgNWs, PVA, and chitosan. The as-achieved TENG had a three-dimensional layered porous structure (Fig. 12a) with great pressure sensitivity (0.3086 V $kPa^{-1}$) and impressive breathability (10.32 kg $m^{-2}$ $d^{-1}$). Besides, the device can be adopted as a skin array (2 × 3) to realize self-powered sensing in volleyball reception statistics (open-circuit voltage up to 130 km $h^{-1}$).[270] Three-layer PVDF/PU/carbon nanofibers have been employed to fabricate a breathable TENG. The all-nanofibre structure showed excellent gas-permeability (10.26 kg $m^{-2}$ $d^{-1}$). This device was utilized for real-time spatial mapping. In short, visible LED signals can be generated from a finger touch on the board (Fig. 12b). In addition, this fibre-based TENG was attached to a hand and acted as a self-sufficient tactile sensor. The single sensor unit (4 × 4 $cm^2$) can be driven by manual hand-tapping with a voltage signal of up to 220 V (Fig. 12c).[87] Fabrics with compelling features of being lightweight, breathable and flexible provide a novel way of fabricating breathable skin-mountable energy-harvesting devices.[271,272] For instance, Qiu *et al.* reported a breathable and tailorable TENG, which was composed of PVDF nanofibres, PET fabrics, and polytetrafluoroethylene nanoparticles by an electrospinning and electrospray technique (Fig. 12d). Due to its porous structure, this device exhibited impressive breathability (8.837 kg $m^{-1}$ $d^{-1}$) (Fig. 12e). The power-generating fabrics were directly integrated into garments (6 cm × 8 cm). The TENG produced an open-circuit voltage of 94.8 V and a current of 1.9 μA when a person walked or stepped naturally.

Published on 03 oajagemánnu 2023. Downloaded on 2026-05-06 16:33:29.

Table 3 Summary of breathable skin-mountable pressure sensors in the last five years

| Materials | Breathability | Sensitivity | Durability | Detection range | Ref. |
|---|---|---|---|---|---|
| Cu/PVA | 25 g $m^{-2}$ $h^{-1}$ | 0.006 $kPa^{-1}$ | — | 0–100 kPa | 101 |
| CNTs/CB/PDMS/CIP | 10.9375 mg $cm^{-2}$ $h^{-1}$ | −0.0198 $kPa^{-1}$ | 10 000 cycles (150 kPa) | 0–200 kPa | 237 |
| PU/CNTs | 357.3 g $m^{-2}$ $d^{-1}$ | 51.53 $kPa^{-1}$ | 8000 cycles (3 kPa) | 0–16 kPa | 126 |
| PVP/PPy/PAN | 1008 g $m^{-2}$ $d^{-1}$ | 4.4 $kPa^{-1}$–11.5 $kPa^{-1}$ | 1500 cycles (0.5 kPa) | 0–20 kPa | 247 |
| Ionic liquid/TPU | 88% water remaining after 60 min | 6.21 $kPa^{-1}$ | 6000 cycles (25.5 kPa) | 23–120 kPa | 248 |
| MXene/silk fibroin nanofibre | — | 298.4 $kPa^{-1}$ | 10 000 cycles (7142 Pa) | 89 Pa–39.28 kPa | 249 |
| AgNWs/PVA/PLGA | 120 mm $s^{-1}$ | 0.011 $kPa^{-1}$ | 50 000 cycles (40 N) | 0–50 kPa | 170 |
| PCBDA/AgNPs/CFN | 25.48 mm $s^{-1}$ | — | 1000 cycles (a human body weight) | 0–400 kPa | 250 |
| TPU/AgNWs | 7.56 $cm^3$ $s^{-1}$ $cm^{-2}$ | 8.31 $kPa^{-1}$ | 10 000 cycles (bending angle of 40°) | 0.5 Pa–80 kPa | 76 |
| C-MOF/polyaniline/PU | 50% water remaining (7 days) | 158.26 $kPa^{-1}$ | 15 000 cycles (3 kPa) | 0–60 kPa | 251 |
| KC/SPP/KC | Mass increased 0.42 g in 7 days | 2.54 $kPa^{-1}$ | >2000 cycles (53 kPa) | 0–165.3 kPa | 252 |
| PDMS/CNTs | — | 0.213 $kPa^{-1}$ | 1000 cycles | 0–12 kPa | 198 |
| AgNWs/TPU | 138 mm $s^{-1}$ | 7.24 $kPa^{-1}$ | 1000 cycles (0.125 kPa) | $9.0 \times 10^{-3}$–0.98 kPa | 253 |
| MXene/nonwoven fabric | 1476.9 mm $s^{-1}$ | 31.40 $kPa^{-1}$ | 1500 cycles (1 kPa) | 0–80 kPa | 104 |
| Cowskin/Pyrrole | 1087 g $m^{-2}$ $d^{-1}$ | 0.144 $kPa^{-1}$ | 15 000 cycles (1.3 kPa) | 0.027–2.72 kPa | 254 |
| MXene/PVDF | 30% water remaining after 8 days | 1970.65 $kPa^{-1}$ | 10 000 cycles (0.95 kPa) | 25 Pa–30 kPa | 89 |
| AgNWs fabric/Ecoflex | 245.58 g $m^{-2}$ $h^{-1}$ | 58 $kPa^{-1}$ | >27 500 cycles (0.9 kPa) | 2.7 Pa–2.3 kPa | 255 |
| $TiO_2$/PVDF/PVA | 57.6% water contented at 65 °C for 48 h | 4.4 $kPa^{-1}$ | 50 000 cycles (1 kPa) | <0.8 Pa | 256 |

PPy polypyrrole, PAN polyacrylonitrile, CIP carbonyl iron particles, PVP polyvinylpyrrolidone, PLGA polylactic-*co*-glycolic acid, KC/SPP/KC K-carrageenan/silk fibroin poly(lactic-coglycolic acid) polyaniline (PANI)/K-carrageenan, C-MOF carbonized metalorganic framework, PCBDA/AgNPs/CFN poly(carboxybetaine-*co*-dopaminemethacrylamide) copolymers/silver nanoparticles/collagen fibre network.

The porous TENG was successfully used as a human motion sensor to monitor the amplitude of movements and postures. When the human arm moved upwards at different angles (15°–90°), the output current increased from 0.5 μA to 1.4 μA, and the output voltage also increased from 41.04 V to 113.21 V (Fig. 12f).[263]

In addition, a breathable paper-based TENG was developed by Yang *et al.* Air-laid paper was successfully utilized as the packed substrate for the TENG, which was composed of PVDF nanofilms and multi-walled CNTs. Based on the punched paper electrodes, air permeability (35.7 mm $s^{-1}$) of the paper-based TENG was greatly improved, while 96% output voltage and 94% output current was retained.[264]

### 4.6. Energy storage devices

Regarding breathable skin-mountable energy storage devices, supercapacitors and batteries are the two most prominent representatives.[273,274] Supercapacitors that have excellent electrochemical properties (*e.g.*, fast charging speed, high energy densities, and long cycle life) are widely used in new energy and the Internet of Things.[277,278] For example, Xu *et al.* reported ultrathin (6 μm) freestanding $MnO_2$–Au–Ni mesh electrodes. The mesh electrodes were further assembled into all-solid-state symmetric supercapacitors with attractive air permeability (45.4 mm $s^{-1}$, 100 Pa), superior electrochemical performances (21.25 mF $cm^{-2}$), and excellent durability (90.1% capacitance retention after 10 000 cycles).[55] Paper-based electrodes were fabricated by depositing CNTs and aqueous PU on dust-free paper using a simple spray technique. The TENG and supercapacitors were made by the airflow mesh structure of the paper electrodes (Fig. 13a). The resultant supercapacitors exhibited excellent breathability (333 mm $s^{-1}$) due to their porous structures. The relationship between the CNTs' coating layers and the permeability is shown in Fig. 13b. After 20 cycles of coating, the electrodes still maintained a permeability of 214 mm $s^{-1}$ and a resistance of only 1.2 Ω $sq^{-1}$. The typical capacitance behaviours at different scan rates showed excellent cycling stability, with no significant change in the cycling voltammetry (CV) curve at 50 mV $s^{-1}$ after 20 000 cycles (Fig. 13c).[275]

Batteries, the most common form of mobile power, have been widely applied in intelligent electronics of different sizes owing to their continuous, stable, and long-term operation.[279] There are two typical breathable skin-mountable batteries: lithium-ion batteries and sweat-activated batteries. Lithium-ion batteries have gained extensive attention because of their immense energy density and low self-discharge.[280,281] For example, based on a carbon cloth-based substrate and a PVA-$LiNO_3$ gel polymer electrolyte, a quasi-solid-state aqueous lithium-ion battery was reported. This battery exhibited impressive cycling stability (79.8% capacity at 0.5 A $g^{-1}$ retention after 500 cycles), which was attributed to the protective polypyrrole coating layers on the $LiNO_3$ and the solid gel polymer electrolyte. The permeability of the lithium-ion battery was achieved by punching hundreds of tiny through-holes in the device.[282] A breathable wood-derived cathode for a lithium–oxygen battery was fabricated by Song *et al.* Inspired by natural wood, this breathable cathode had a 3D layered

 This journal is © The Royal Society of Chemistry 2023

Published on 03 oajagemännu 2023. Downloaded on 2026-05-06 16:33:29.

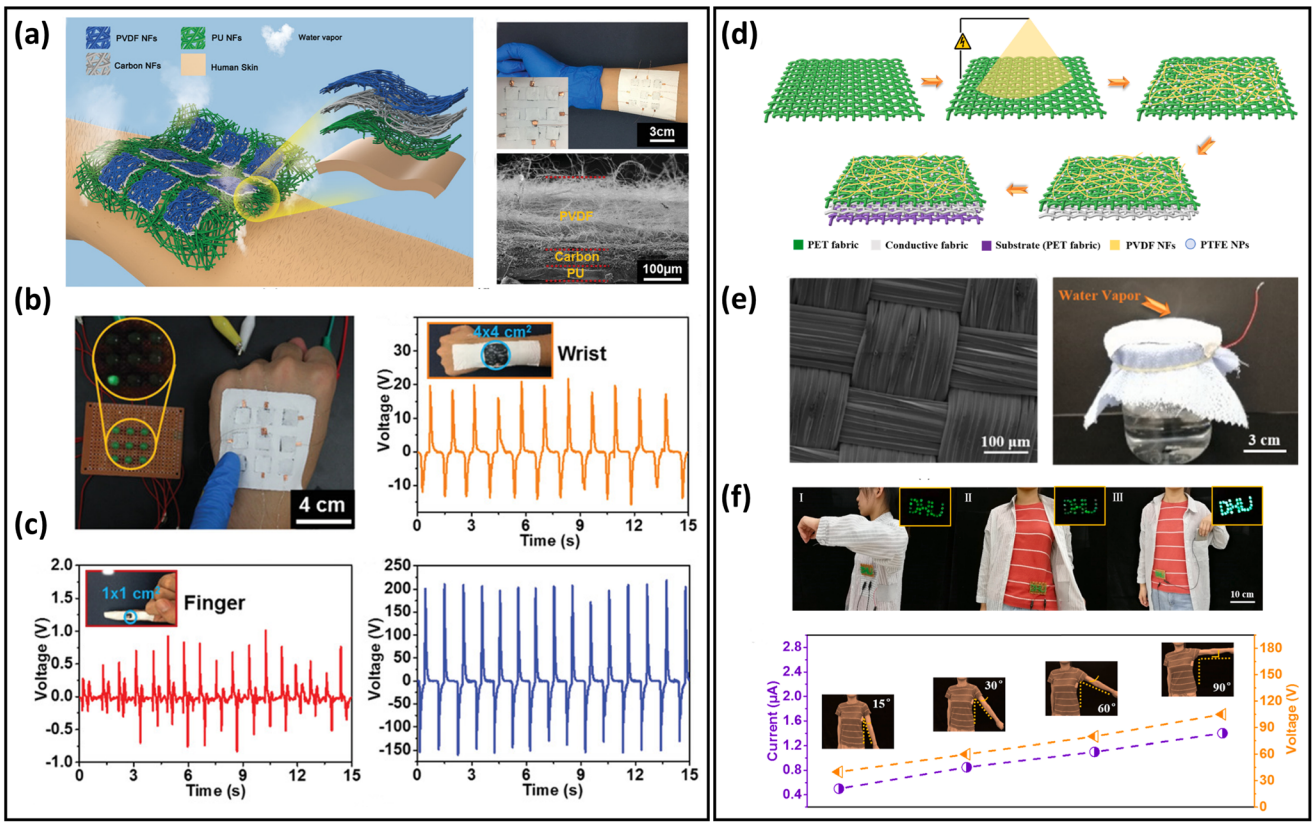


**Fig. 12** Breathable skin-mountable energy harvesting devices. (a) Schematic diagram of the all-fibre-based TENG. The inset shows a partial magnification of a single sensor attached to the arm and an SEM image of a cross-section of the TENG. (b) TENG maps different touch events on the wrist and biomechanical energy harvesting from a single wrist. (c) Human biomechanical energy and voltage signals are collected from a single TENG attached to a human finger. Reproduced with permission from ref. 87. Copyright 2019 Wiley-VCH. (d) Schematic diagram of the fabrication of the power-generation fabric. (e) SEM image of conductive fabric and demonstration of breathability of power-generation fabric. (f) Current and voltage output of the power-generating fabric as the human arm was moved upwards at different angles. Reproduced with permission from ref. 263. Copyright 2022 Elsevier.

porous structure with a thickness of 700 μm. The assembled Li–$O_2$ batteries exhibited excellent areal specific capacity (8.58 mA h $cm^{-2}$) at 0.1 mA $cm^{-2}$.[283]

Sweat-activated batteries are also considered to be a promising energy supply candidate.[284,285] For instance, Liu *et al.* reported an ultrathin breathable bandage-based sweat-activated battery, composed of two encapsulation PDMS layers (the top layer of 0.8 mm and bottom layer of 1.6 mm) and a series of electronic components.[276] The Ni/graphene foam sweat-activated battery was attached to human skin *via* a bandage, with breathable sports tape (0.3 mm) for air exchange. The graphene coating was stored in the foam metal to increase the strength of the redox (Fig. 13d). Besides, the flexible sweat-activated battery generated a high capacity of 74.4 mA h (Fig. 13e). The generated energy can be utilized to continuously illuminate 120 LEDs for over 4 h and monitor ECG, EMG for more than 1.2 h (Fig. 13f).

In addition to Li-ion batteries and sweat-activated batteries, other batteries such as Na–$O_2$ batteries and Zn–air batteries have also been used to develop breathable skin-mountable energy storage devices.[286–288] For example, by 3D printing of hierarchical porous structures for rGO air electrodes, Na–$O_2$ permeable batteries were fabricated. Na–$O_2$ batteries using "$O_2$ breathable" electronics achieved a high capacity of 13 484.6 mA h $g^{-1}$ at 0.2 A $g^{-1}$ and an excellent cycling performance (120 cycles with a cutoff capacity of 500 mA h $g^{-1}$ at 0.5 A $g^{-1}$).

### 4.7. Others

Other applications of breathable skin-mountable electronics include actuators,[289–291] chemical sensors,[292–294] solar cells,[7] and organic electrochemical transistors,[133] *etc.* For example, Chen *et al.* developed an organic chemical transistor using electrospun PVDF-hexafluoropropylene as the ionic polymer matrix and 1-ethyl-3-methylimidazolium bis(trifluoromethylsulfonyl)amide as the ionic source. Then, the authors deposited Au electrode and spray-coated PEDOT:PSS layer on the fibrous membrane. To evaluate its gas permeability, the weight loss of water in a bottle before and after covering with hybrid films was measured. The results showed that the difference in WVTR was negligible. The fibrous organic chemical transistor electrodes have been successfully utilized for long-term health-

Published on 03 oajagemánnu 2023. Downloaded on 2026-05-06 16:33:29.

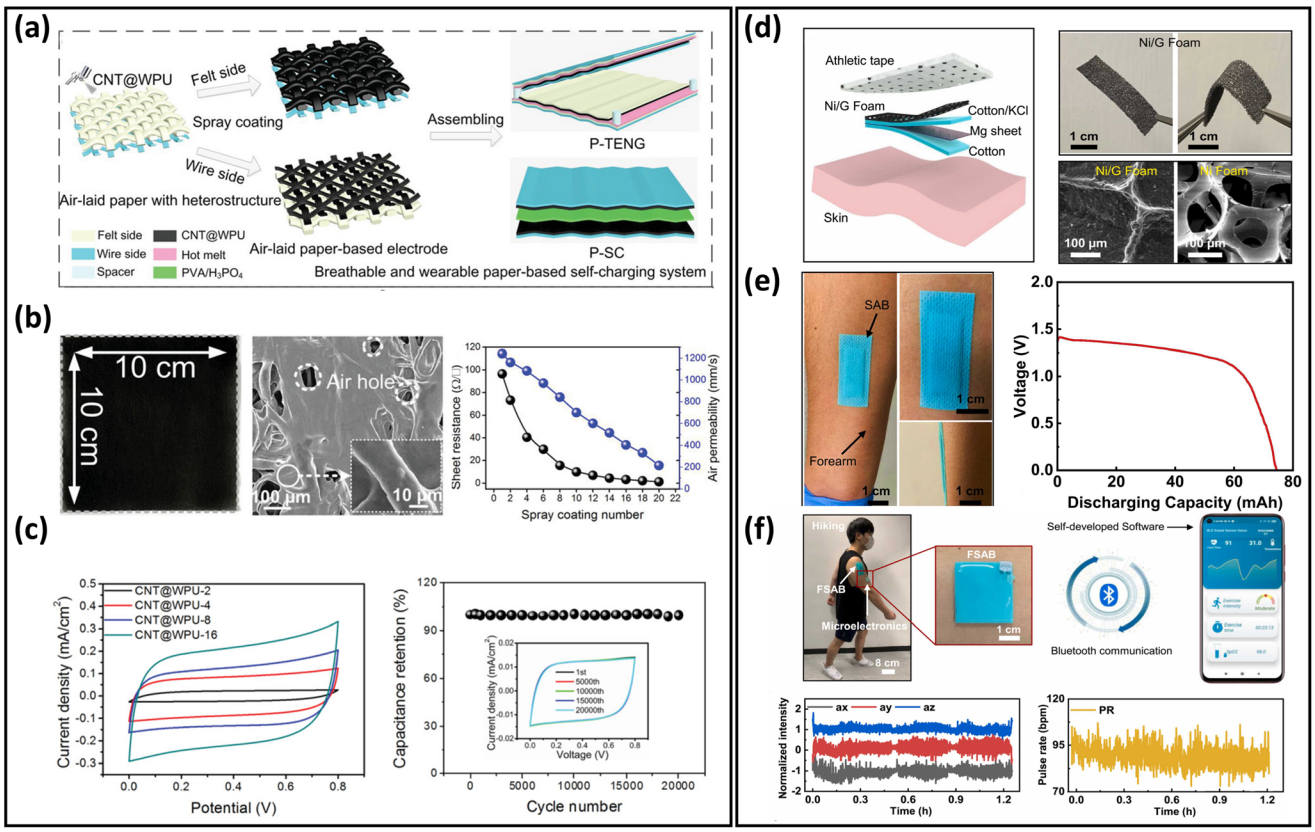


**Fig. 13** Breathable skin-mountable energy storage devices. (a) Schematic diagram of the fabrication of TENG and supercapacitor based on air-laid paper. (b) Images and SEM images of paper electrodes, and sheet resistance and air permeability of paper electrodes with different coating times. (c) CV curves and cycle performance of CNTs@WPU supercapacitor. Reproduced with permission from ref. 275. Copyright 2019 Wiley-VCH. (d) Schematic diagram of a sweat-activated battery. Optical images and SEM images of graphene-coated nickel foam. (e) Optical images of a sweat-activated battery mounted on a human forearm. Power density *versus* voltage of the sweat-activated battery under constant conditions. (f) The optical image of the entire system during movement with Bluetooth wireless real-time monitoring of human physiological signals. Reproduced with permission from ref. 276. Copyright 2022 Elsevier.

care monitoring, with excellent stability of the ECG signals (21.7 dB) during 1 week.[133] A breathable PVA-poly(4-styrenesulphonic acid)-GO film alcohol fuel cell sensor was fabricated by a simple solution casting method. Due to the porous structure, the film sensor exhibited great permeability. The sensor had excellent electrical properties with conductivities of 0.13 S $cm^{-1}$ (in-plane) and 22.6 S $cm^{-1}$ (out-of-plane) at 75 °C. Meanwhile, this semi-penetrating network-assembled alcohol fuel sensor exhibited a low ethanol-monitoring limit (25 ppm) and excellent water retention.[295] Nayeem *et al.* reported an all-nanofibre mechanoacoustic sensor based on electrospun PU/PVDF. The all-fibre structures of the sensor showed excellent permeability (12.4 kg $m^{-2}$ $d^{-1}$) and high sensitivity of 10 050.6 mV $Pa^{-1}$ in the low-frequency region (<500 Hz). In addition, the breathable mechanoacoustic sensor could be utilized to continuously measure the heart signals with an SNR of up to 40.9 dB over 10 h.[179] An ultralight (1.25 mg $cm^{-2}$) glucose-monitoring patch was fabricated by depositing $Cu_2O$ (glucose biorecognition element) onto a Ni micromesh. This glucose biosensor showed an impressive gas permeability (>2500 mm $s^{-1}$ at 10 Pa). The resulting glucose-monitoring electrodes exhibited excellent glucose-detection responses including high sensitivity (15 420 μA $cm^{-2}$ $mM^{-1}$) and low detection limit (50 nM).[296]

Multifunctionality and robust sensing types are important research directions to develop high-performance permeable skin-mountable electronics.[297–299] For instance, Liang *et al.* reported a breathable graphene decorated textile multimodal smart wearable system. This device can successfully monitor strain and biopotential signals at the same time.[100]

## 5. Conclusions and prospects

In this report, we comprehensively review recent advances in breathable skin-mountable electronics. First, materials and structure strategies are described in detail, including ultrathin materials and devices, electrospun nanofibre-based, yarn/fabric-based, and structure design. Then, we discuss five device properties, *i.e.*, breathability, biocompatibility, adhesion, stretchability, and long-term usage. Finally, we present representative applications of breathable skin-mounta-

 This journal is © The Royal Society of Chemistry 2023

Published on 03 oajagemánnu 2023. Downloaded on 2026-05-06 16:33:29.

ble electronics, such as bioelectrical sensors, temperature sensors, humidity and hydration sensors, strain and pressure sensors, energy harvesting and storage devices, *etc.* Despite much progress achieved in this field, there are still challenges in the following directions that await further development. In the following part, we outline several remaining challenges with pertinent solutions.

### 5.1 Material and structure design

Despite numerous developments in porous materials and devices, such as ultrathin materials and devices, electrospun nanofibre-based, yarn/fibre-based, and structure designs, breathable skin-mountable electronics are still underdeveloped due to uncontrollable pore structure and poor sample consistency. Advanced fabrication and assembling techniques, such as spinning and printing, are necessary to achieve uniform porous materials and devices. Representative approaches for device structures in gas-permeable skin-mountable electronics include ultrathin and porous form factors.[24] However, if a device is thin enough to realise breathability, the mechanical properties are usually weak. Similarly, a porous-designed breathable electronic device is usually thick and layered-based, leading to limited skin compliance. Therefore, novel materials and structure designs are required to overcome these trade-offs. For example, reinforced materials can be considered for ultrathin design, and adhesive materials for porous design, to fabricate high-performance breathable skin-mountable electronic devices.

### 5.2 Multifunctional integration

The ultimate goal of breathable skin-mountable electronics is to develop a closed-loop system that can operate autonomously and efficiently. In recent years, laboratory research has prepared tremendous high-performance sensors and energy devices for physiological monitoring, energy harvesting and storage; most of these are single device-based platforms. However, research in multifunction integration is still lacking. Future research will require the integration of various gas-permeable sensors, energy devices, actuators, *etc.*, in a single platform. Such platforms significantly increase device density and realize multifunctionalities, including self-sustainability and simultaneous monitoring of bioelectrical, biophysical, and biochemical signals. To achieve this, collaborative efforts from experts in materials, electrical, mechanical, and biological engieering are required for technological advancement.[25] Furthermore, the interference between different sensors and energy devices, and the compatibility with the substrate materials of breathable skin-mountable electronics, should be considered.[300]

### 5.3 System intelligence

Nowadays, integrated with artificial intelligence (AI) and machine learning techniques (*e.g.*, artificial neural networks, decision trees and hierarchical cluster analysis), soft electronics can accurately predict prostate cancer,[301] diabetes,[302] Covid-19,[303] *etc.* Breathable skin-mountable electronics are appealing and promissing to enable truly individualized patient care by providing long-term health care applications. However, most breathable skin-mountable electronics are not intelligent, severely limiting their full potential applications in disease analysis and management. Regarding this, advanced data management techniques are necessary to realize the intelligence of breathable sensors and devices, thus providing solutions for clinical decision-making. Despite the excellence of AI algorithms in disease diagnosis, matching AI algorithms with medical expertise remains a challenge. In addition, high-quality data training is also required to build complete disease databases.[304,305]

Despite the existence of unresolved challenges, we believe that with the continued development of all the above aspects, breathable skin-mountable electronics will realize their full potential. In the future, high-performance, integrated, and intelligent breathable skin-mountable electronics are capable of long-term, continuous health care management throughout daily life, promising to revolutionize traditional clinical practices.

## Conflicts of interest

There are no conflicts to declare.

## Acknowledgements

Y. Wang would like to acknowledge support from the Technion, the Li Ka Shing Foundation Cross-disciplinary Research Program (No.: 2022LKSFG12A), Young Talent Innovation Project of Guangdong Education Department, (No.: 2022KQNCX112), Guangdong Science and Technology Department (No.: STKJ202209085), and the Start-up Fund from Guangdong Technion.

## References

1 T. Someya and M. Amagai, *Nat. Biotechnol.*, 2019, **37**, 382–388.
2 C. Wang, C. Wang, Z. Huang and S. Xu, *Adv. Mater.*, 2018, **30**, 1801368.
3 J. C. Yang, J. Mun, S. Y. Kwon, S. Park, Z. Bao and S. Park, *Adv. Mater.*, 2019, **31**, 1904765.
4 W. D. Li, K. Ke, J. Jia, J. H. Pu, X. Zhao, R. Y. Bao, Z. Y. Liu, L. Bai, K. Zhang and M. B. Yang, *Small*, 2022, **18**, 2103734.
5 J. Zhong, Z. Li, M. Takakuwa, D. Inoue, D. Hashizume, Z. Jiang, Y. Shi, L. Ou, M. O. G. Nayeem, S. Umezu, K. Fukuda and T. Someya, *Adv. Mater.*, 2022, **34**, 2107758.
6 Y. Ma, Y. Zhang, S. Cai, Z. Han, X. Liu, F. Wang, Y. Cao, Z. Wang, H. Li and Y. Chen, *Adv. Mater.*, 2020, **32**, 1902062.
7 S. Park, S. W. Heo, W. Lee, D. Inoue, Z. Jiang, K. Yu, H. Jinno, D. Hashizume, M. Sekino and T. Yokota, *Nature*, 2018, **561**, 516–521.
8 K. Fukuda, K. Yu and T. Someya, *Adv. Energy Mater.*, 2020, **10**, 2000765.

Published on 03 oajagemännu 2023. Downloaded on 2026-05-06 16:33:29.

9 M. Choi, S.-R. Bae, L. Hu, A. T. Hoang, S. Y. Kim and J.-H. Ahn, *Sci. Adv.*, 2020, **6**, eabb5898.
10 T. Sekitani, H. Nakajima, H. Maeda, T. Fukushima, T. Aida, K. Hata and T. Someya, *Nat. Mater.*, 2009, **8**, 494–499.
11 A. Miyamoto, S. Lee, N. F. Cooray, S. Lee, M. Mori, N. Matsuhisa, H. Jin, L. Yoda, T. Yokota and A. Itoh, *Nat. Nanotechnol.*, 2017, **12**, 907–913.
12 C. García Núñez, L. Manjakkal and R. Dahiya, *npj Flexible Electron.*, 2019, **3**, 1.
13 D. Kireev, J. Kampfe, A. Hall and D. Akinwande, *npj 2D Mater. Appl.*, 2022, **6**, 46.
14 S. A. Han, J. Lee, J. Lin, S.-W. Kim and J. H. Kim, *Nano Energy*, 2019, **57**, 680–691.
15 G. Mearini, D. Stimpel, B. Geertz, F. Weinberger, E. Krämer, S. Schlossarek, J. Mourot-Filiatre, A. Stoehr, A. Dutsch, P. J. M. Wijnker, I. Braren, H. A. Katus, O. J. Müller, T. Voit, T. Eschenhagen and L. Carrier, *Nat. Commun.*, 2014, **5**, 5515.
16 J. Rocklöv and R. Dubrow, *Nat. Immunol.*, 2020, **21**, 479–483.
17 S. Kafonek, W. H. Ettinger, R. Roca, S. Kittner, N. Taylor and P. S. German, *J. Am. Geriatr. Soc.*, 1989, **37**, 29–34.
18 Y. Lei, B. Yang, X. Jiang, F. Jia, N. Li and A. K. Nandi, *Mech. Syst. Signal Process.*, 2020, **138**, 106587.
19 D. Zhang, Z. Wu and X. Zong, *Sens. Actuators, B*, 2019, **289**, 32–41.
20 C. Hou, Z. Xu, W. Qiu, R. Wu, Y. Wang, Q. Xu, X. Y. Liu and W. Guo, *Small*, 2019, **15**, 1805084.
21 J. Huang, Z. Xu, W. Qiu, F. Chen, Z. Meng, C. Hou, W. Guo and X. Y. Liu, *Adv. Funct. Mater.*, 2020, **30**, 1910547.
22 J. Shao, J. Zhang, N. A. Villasis, X. Li, G. Chen, G. Chen, J. Yu, Y. Zhang, J. Wang, Y. Gao, J. Lin, P. Huang and Z. Gu, *Matter*, 2023, **6**(1), 158–174.
23 K.-I. Jang, S. Y. Han, S. Xu, K. E. Mathewson, Y. Zhang, J.-W. Jeong, G.-T. Kim, R. C. Webb, J. W. Lee and T. J. Dawidczyk, *Nat. Commun.*, 2014, **5**, 1–10.
24 Q. Huang and Z. Zheng, *ACS Nano*, 2022, **16**, 15537–15544.
25 Y. Wang, H. Haick, S. Guo, C. Wang, S. Lee, T. Yokota and T. Someya, *Chem. Soc. Rev.*, 2022, **51**, 3759–3793.
26 B. Arman Kuzubasoglu and S. Kursun Bahadir, *Sens. Actuators, A*, 2020, **315**, 112282.
27 H. Tai, Z. Duan, Y. Wang, S. Wang and Y. Jiang, *ACS Appl. Mater. Interfaces*, 2020, **12**, 31037–31053.
28 J.-w. Zhang, Y. Zhang, Y.-y. Li and P. Wang, *Polym. Rev.*, 2022, **62**, 65–94.
29 M. Zhu, J. Li, J. Yu, Z. Li and B. Ding, *Angew. Chem., Int. Ed.*, 2022, **61**, e202200226.
30 C. Li, R. Cao and X. Zhang, *Appl. Sci.*, 2018, **8**, 2485.
31 Y. Wang, T. Yokota and T. Someya, *NPG Asia Mater.*, 2021, **13**, 1–22.
32 Y. Xu, Q. Fei, M. Page, G. Zhao, Y. Ling, S. B. Stoll and Z. Yan, *iScience*, 2021, **24**, 102736.
33 F. Chen, Q. Huang and Z. Zheng, *Small Struct.*, 2021, **3**, 2100135.
34 X. Xu, S. Xie, Y. Zhang and H. Peng, *Angew. Chem., Int. Ed.*, 2019, **58**, 13643–13653.
35 Z. Yin, H. Lu, L. Gan and Y. Zhang, *Adv. Mater. Technol.*, 2022, 2200654, DOI: **10.1002/admt.202200654**.
36 L. Wei, S. Wang, M. Shan, Y. Li, Y. Wang, F. Wang, L. Wang and J. Mao, *Bioact. Mater.*, 2023, **22**, 343–364.
37 Z. Yin, H. Lu, L. Gan and Y. Zhang, *Adv. Mater. Technol.*, 2022, 220065, DOI: **10.1002/admt.202200654**.
38 Y. Yang, T. Cui, D. Li, S. Ji, Z. Chen, W. Shao, H. Liu and T.-L. Ren, *Nano-Micro Lett.*, 2022, **14**, 161.
39 K.-I. Jang, H. U. Chung, S. Xu, C. H. Lee, H. Luan, J. Jeong, H. Cheng, G.-T. Kim, S. Y. Han and J. W. Lee, *Nat. Commun.*, 2015, **6**, 1–11.
40 J. Chen, Y. Huang, N. Zhang, H. Zou, R. Liu, C. Tao, X. Fan and Z. L. Wang, *Nat. Energy*, 2016, **1**, 1–8.
41 A. Miyamoto, S. Lee, N. F. Cooray, S. Lee, M. Mori, N. Matsuhisa, H. Jin, L. Yoda, T. Yokota, A. Itoh, M. Sekino, H. Kawasaki, T. Ebihara, M. Amagai and T. Someya, *Nat. Nanotechnol.*, 2017, **12**, 907–913.
42 Y. J. Fan, X. Li, S. Y. Kuang, L. Zhang, Y. H. Chen, L. Liu, K. Zhang, S. W. Ma, F. Liang, T. Wu, Z. L. Wang and G. Zhu, *ACS Nano*, 2018, **12**, 9326–9332.
43 L. Tian, B. Zimmerman, A. Akhtar, K. J. Yu, M. Moore, J. Wu, R. J. Larsen, J. W. Lee, J. Li, Y. Liu, B. Metzger, S. Qu, X. Guo, K. E. Mathewson, J. A. Fan, J. Cornman, M. Fatina, Z. Xie, Y. Ma, J. Zhang, Y. Zhang, F. Dolcos, M. Fabiani, G. Gratton, T. Bretl, L. J. Hargrove, P. V. Braun, Y. Huang and J. A. Rogers, *Nat. Biomed. Eng.*, 2019, **3**, 194–205.
44 Y. Wang, S. Lee, T. Yokota, H. Wang, Z. Jiang, J. Wang, M. Koizumi and T. Someya, *Sci. Adv.*, 2020, **6**, eabb7043.
45 Z. Ma, Q. Huang, Q. Xu, Q. Zhuang, X. Zhao, Y. Yang, H. Qiu, Z. Yang, C. Wang and Y. Chai, *Nat. Mater.*, 2021, **20**, 859–868.
46 G. Gwon, H. Choi, J. Bae, N. A. B. Zulkifli, W. Jeong, S. Yoo, D. C. Hyun and S. Lee, *Adv. Funct. Mater.*, 2022, **32**, 2204645.
47 Y. Won, J. J. Lee, J. Shin, M. Lee, S. Kim and S. Gandla, *ACS Sens.*, 2021, **6**, 967–975.
48 Y. Fang, Y. Li, Y. Li, M. Ding, J. Xie and B. Hu, *ACS Appl. Mater. Interfaces*, 2020, **12**, 23689–23696.
49 Y. Wang, S. Lee, H. Wang, Z. Jiang, Y. Jimbo, C. Wang, B. Wang, J. J. Kim, M. Koizumi, T. Yokota and T. Someya, *Proc. Natl. Acad. Sci. U. S. A.*, 2021, **118**, e2111904118.
50 Q. Li, G. Chen, Y. Cui, S. Ji, Z. Liu, C. Wan, Y. Liu, Y. Lu, C. Wang, N. Zhang, Y. Cheng, K.-Q. Zhang and X. Chen, *ACS Nano*, 2021, **15**, 9955–9966.
51 T. Q. Trung, H. S. Le, T. M. L. Dang, S. Ju, S. Y. Park and N.-E. Lee, *Adv. Healthcare Mater.*, 2018, **7**, 1800074.
52 W. Zhou, S. Yao, H. Wang, Q. Du, Y. Ma and Y. Zhu, *ACS Nano*, 2020, **14**, 5798–5805.
53 S. Kabiri Ameri, R. Ho, H. Jang, L. Tao, Y. Wang, L. Wang, D. M. Schnyer, D. Akinwande and N. Lu, *ACS Nano*, 2017, **11**, 7634–7641.
54 L. Hu, H. S. Kim, J.-Y. Lee, P. Peumans and Y. Cui, *ACS Nano*, 2010, **4**, 2955–2963.


This journal is © The Royal Society of Chemistry 2023

Published on 03 oajagemánnu 2023. Downloaded on 2026-05-06 16:33:29.

55 J.-L. Xu, Y.-H. Liu, X. Gao, S. Shen and S.-D. Wang, *Energy Storage Mater.*, 2019, **22**, 402–409.
56 Y. Li, Z. Xu, L. Chen and Y. Liu, *Adv. Sens. Syst. Appl. X*, 2020, **11554**, 218–225.
57 K. K. Kim, S. Hong, H. M. Cho, J. Lee, Y. D. Suh, J. Ham and S. H. Ko, *Nano Lett.*, 2015, **15**, 5240–5247.
58 S. Jeong, H. Cho, S. Han, P. Won, H. Lee, S. Hong, J. Yeo, J. Kwon and S. H. Ko, *Nano Lett.*, 2017, **17**, 4339–4346.
59 Y. Wang, J. Wang, S. Cao and D. Kong, *J. Mater. Chem. C*, 2019, **7**, 9748–9755.
60 P. Won, J. J. Park, T. Lee, I. Ha, S. Han, M. Choi, J. Lee, S. Hong, K.-J. Cho and S. H. Ko, *Nano Lett.*, 2019, **19**, 6087–6096.
61 C. Cho, W. Shin, M. Kim, J. Bang, P. Won, S. Hong and S. H. Ko, *Small*, 2022, **18**, 2202841.
62 I. Hong, S. Lee, D. Kim, H. Cho, Y. Roh, H. An, S. Hong, S. H. Ko and S. Han, *Nanotechnology*, 2019, **30**, 074001.
63 D. Kim, J. Bang, W. Lee, I. Ha, J. Lee, H. Eom, M. Kim, J. Park, J. Choi, J. Kwon, S. Han, H. Park, D. Lee and S. H. Ko, *J. Mater. Chem. A*, 2020, **8**, 8281–8291.
64 K. Qiu, A. Elhassan, T. Tian, X. Yin, J. Yu, Z. Li and B. Ding, *ACS Appl. Mater. Interfaces*, 2020, **12**, 11016–11025.
65 J. Bang, Y. Jung, H. Kim, D. Kim, M. Cho and S. H. Ko, *Nano-Micro Lett.*, 2022, **14**, 49.
66 S. Han, J. Kim, Y. Lee, J. Bang, C. G. Kim, J. Choi, J. Min, I. Ha, Y. Yoon, C.-H. Yun, M. Cruz, B. J. Wiley and S. H. Ko, *Nano Lett.*, 2022, **22**, 524–532.
67 Q. Cao and J. A. Rogers, *Adv. Mater.*, 2009, **21**, 29–53.
68 V. Schroeder, S. Savagatrup, M. He, S. Lin and T. M. Swager, *Chem. Rev.*, 2018, **119**, 599–663.
69 J. Cui, F. Li, Y. Wang, Q. Zhang, W. Ma and C. Huang, *Sep. Purif. Technol.*, 2020, **250**, 117116.
70 X. Wang, W.-Z. Song, M.-H. You, J. Zhang, M. Yu, Z. Fan, S. Ramakrishna and Y.-Z. Long, *ACS Nano*, 2018, **12**, 8588–8596.
71 H. Wu, D. Kong, Z. Ruan, P.-C. Hsu, S. Wang, Z. Yu, T. J. Carney, L. Hu, S. Fan and Y. Cui, *Nat. Nanotechnol.*, 2013, **8**, 421–425.
72 J. Xue, T. Wu, Y. Dai and Y. Xia, *Chem. Rev.*, 2019, **119**, 5298–5415.
73 Z. Sun, L. Feng, C. Xiong, X. He, L. Wang, X. Qin and J. Yu, *J. Mater. Chem. A*, 2021, **9**, 7085–7093.
74 K. Qi, Y. Zhou, K. Ou, Y. Dai, X. You, H. Wang, J. He, X. Qin and R. Wang, *Carbon*, 2020, **170**, 464–476.
75 Y. Gao, F. Guo, P. Cao, J. Liu, D. Li, J. Wu, N. Wang, Y. Su and Y. Zhao, *ACS Nano*, 2020, **14**, 3442–3450.
76 P. Yu, X. Li, H. Li, Y. Fan, J. Cao, H. Wang, Z. Guo, X. Zhao, Z. Wang and G. Zhu, *ACS Appl. Mater. Interfaces*, 2021, **13**, 24062–24069.
77 A. Rajak, D. A. Hapidin, F. Iskandar, M. M. Munir and K. Khairurrijal, *Waste Manage.*, 2020, **103**, 76–86.
78 Y. Li, J. Xiong, J. Lv, J. Chen, D. Gao, X. Zhang and P. S. Lee, *Nano Energy*, 2020, **78**, 105358.
79 C. Altinkok, H. F. Karabulut, M. A. Tasdelen and G. Acik, *Mater. Today Commun.*, 2020, **25**, 101425.
80 J.-H. Zhang, Z. Li, J. Xu, J. Li, K. Yan, W. Cheng, M. Xin, T. Zhu, J. Du, S. Chen, X. An, Z. Zhou, L. Cheng, S. Ying, J. Zhang, X. Gao, Q. Zhang, X. Jia, Y. Shi and L. Pan, *Nat. Commun.*, 2022, **13**, 5839.
81 A. Babu, I. Aazem, R. Walden, S. Bairagi, D. M. Mulvihill and S. C. Pillai, *Chem. Eng. J.*, 2023, **452**, 139060.
82 G.-M. Lanno, C. Ramos, L. Preem, M. Putrins, I. Laidmae, T. Tenson and K. Kogermann, *ACS Omega*, 2020, **5**, 30011–30022.
83 M. Sheikholeslam, M. E. Wright, N. Cheng, H. H. Oh, Y. Wang, A. K. Datu, J. P. Santerre, S. Amini-Nik and M. G. Jeschke, *ACS Biomater. Sci. Eng.*, 2019, **6**, 505–516.
84 Z. Jiang, M. O. G. Nayeem, K. Fukuda, S. Ding, H. Jin, T. Yokota, D. Inoue, D. Hashizume and T. Someya, *Adv. Mater.*, 2019, **31**, 1903446.
85 C. Lang, J. Fang, H. Shao, X. Ding and T. Lin, *Nat. Commun.*, 2016, **7**, 11108.
86 J. Huang, Y. Hao, M. Zhao, W. Li, F. Huang and Q. Wei, *ACS Appl. Mater. Interfaces*, 2021, **13**, 24774–24784.
87 Z. Li, M. Zhu, J. Shen, Q. Qiu, J. Yu and B. Ding, *Adv. Funct. Mater.*, 2019, **30**, 1908411.
88 H. Zhai, L. Xu, Z. Liu, L. Jin, Y. Yi, J. Zhang, Y. Fan, D. Cheng, J. Li, X. Liu, Q. Song, P. Yue and Y. Li, *Chem. Eng. J.*, 2022, **439**, 135502.
89 W. Du, Z. Li, Y. Zhao, X. Zhang, L. Pang, W. Wang, T. Jiang, A. Yu and J. Zhai, *Chem. Eng. J.*, 2022, **446**, 137268.
90 J. Chen, F. Wang, G. Zhu, C. Wang, X. Cui, M. Xi, X. Chang and Y. Zhu, *ACS Appl. Mater. Interfaces*, 2021, **13**, 51567–51577.
91 P. Wang, W. Yu, G. Li, C. Meng and S. Guo, *Chem. Eng. J.*, 2023, **452**, 139174.
92 I. Marriam, X. Wang, M. Tebyetekerwa, G. Chen, F. Zabihi, J. Pionteck, S. Peng, S. Ramakrishna, S. Yang and M. Zhu, *J. Mater. Chem. A*, 2018, **6**, 13633–13643.
93 Z. Yin, M. Jian, C. Wang, K. Xia, Z. Liu, Q. Wang, M. Zhang, H. Wang, X. Liang and X. Liang, *Nano Lett.*, 2018, **18**, 7085–7091.
94 J. Zhao, Y. Fu, Y. Xiao, Y. Dong, X. Wang and L. Lin, *Adv. Mater. Technol.*, 2019, **5**, 1900781.
95 H. Li, S. Zhao, X. Du, J. Wang, R. Cao, Y. Xing and C. Li, *Adv. Mater. Technol.*, 2018, **3**, 1800065.
96 M. Lou, I. Abdalla, M. Zhu, X. Wei, J. Yu, Z. Li and B. Ding, *ACS Appl. Mater. Interfaces*, 2020, **12**, 19965–19973.
97 M. Pasta, F. La Mantia, L. Hu, H. D. Deshazer and Y. Cui, *Nano Res.*, 2010, **3**, 452–458.
98 L. V. Thekkekara and M. Gu, *Sci. Rep.*, 2019, **9**, 11822.
99 M. Sala de Medeiros, D. Chanci, C. Moreno, D. Goswami and R. V. Martinez, *Adv. Funct. Mater.*, 2019, **29**, 1904350.
100 X. Liang, M. Zhu, H. Li, J. Dou, M. Jian, K. Xia, S. Li and Y. Zhang, *Adv. Funct. Mater.*, 2022, **32**, 2200162.
101 Z. Liu, Y. Zheng, L. Jin, K. Chen, H. Zhai, Q. Huang, Z. Chen, Y. Yi, M. Umar, L. Xu, G. Li, Q. Song, P. Yue, Y. Li and Z. Zheng, *Adv. Funct. Mater.*, 2021, **31**, 2007622.
102 X. Zhang, J. Wang, Y. Xing and C. Li, *Glob. Chall.*, 2019, **3**, 1900070.

Published on 03 oajagemännu 2023. Downloaded on 2026-05-06 16:33:29.

103 Y.-E. Shin, J.-E. Lee, Y. Park, S.-H. Hwang, H. G. Chae and H. Ko, *J. Mater. Chem. A*, 2018, **6**, 22879–22888.
104 G. Sun, P. Wang, Y. Jiang, H. Sun and C. Meng, *ACS Appl. Electron. Mater.*, 2022, **4**, 1958–1967.
105 C. Chen, L. Chen, Z. Wu, H. Guo, W. Yu, Z. Du and Z. L. Wang, *Mater. Today*, 2020, **32**, 84–93.
106 J. Wen, B. Xu and J. Zhou, *Nano-Micro Lett.*, 2019, **11**, 1–14.
107 N. Karim, S. Afroj, A. Malandraki, S. Butterworth, C. Beach, M. Rigout, K. S. Novoselov, A. J. Casson and S. G. Yeates, *J. Mater. Chem. C*, 2017, **5**, 11640–11648.
108 Ö. Özen, D. Yilmaz and K. Yapici, *Cellulose*, 2022, **29**, 4767–4785.
109 R. Yang, Y. Xu, C. Xie and H. Wang, *Dyes Pigm.*, 2019, **165**, 151–156.
110 Y. Jang, S. M. Kim, G. M. Spinks and S. J. Kim, *Adv. Mater.*, 2020, **32**, 1902670.
111 S. Praveen, G. S. Sim, C. W. Ho and C. W. Lee, *Energy Storage Mater.*, 2021, **41**, 748–757.
112 M. Bar, R. Alagirusamy and A. Das, *Compos. Struct.*, 2018, **197**, 63–71.
113 X. Tao, Y. Zhou, K. Qi, C. Guo, Y. Dai, J. He and Z. Dai, *J. Colloid Interface Sci.*, 2022, **608**, 2339–2346.
114 Y. Gao, Z. Li, B. Xu, M. Li, C. Jiang, X. Guan and Y. Yang, *Nano Energy*, 2022, **91**, 106672.
115 D. Zhang, W. Yang, W. Gong, W. Ma, C. Hou, Y. Li, Q. Zhang and H. Wang, *Adv. Mater.*, 2021, **33**, 2100782.
116 Q. Gao, T. Lauster, B. A. F. Kopera, M. Retsch, S. Agarwal and A. Greiner, *Adv. Funct. Mater.*, 2022, **32**, 2108808.
117 G. Yang, R. Xing, Y. Li, C. Ma, B. Cheng, J. Yan and X. Zhuang, *Chem. Eng. J.*, 2021, **426**, 131931.
118 H. Liu, X. Zhong, X. He, Y. Li, N. Zhou, Z. Ma, D. Zhu and H. Ji, *ACS Appl. Mater. Interfaces*, 2021, **13**, 55656–55665.
119 L. Xu, Z. Liu, X. Chen, R. Sun, Z. Hu, Z. Zheng, T. T. Ye and Y. Li, *Adv. Intell. Syst.*, 2019, **1**, 1900056.
120 Y. Cho, G. T. Nguyen, Q. V. Duong and S. T. Choi, *J. Mech. Sci. Technol.*, 2022, **36**, 3573–3584.
121 H. M. Lee, S. Y. Choi, A. Jung and S. H. Ko, *Angew. Chem.*, 2013, **125**, 7872–7877.
122 D. Wang, J. Sun, Q. Xue, Q. Li, Y. Guo, Y. Zhao, Z. Chen, Z. Huang, Q. Yang, G. Liang, B. Dong and C. Zhi, *Energy Storage Mater.*, 2021, **36**, 272–278.
123 X. Wang, C. Yan, H. Hu, X. Zhou, R. Guo, X. Liu, Z. Xie, Z. Huang and Z. Zheng, *Chem. – Asian J.*, 2014, **9**, 2170–2177.
124 Y. Atwa, N. Maheshwari and I. A. Goldthorpe, *J. Mater. Chem. C*, 2015, **3**, 3908–3912.
125 H. Min, S. Jang, D. W. Kim, J. Kim, S. Baik, S. Chun and C. Pang, *ACS Appl. Mater. Interfaces*, 2020, **12**, 14425–14432.
126 Y. He, L. Zhao, J. Zhang, L. Liu, H. Liu and L. Liu, *Compos. Sci. Technol.*, 2020, **200**, 108419.
127 L. You, X. Shi, J. Cheng, J. Yang, C. Xiong, Z. Ding, Z. Zheng, S. Wang and J. Wang, *J. Colloid Interface Sci.*, 2022, **625**, 197–209.
128 M. Xu, Y. Wang, F. Chen, J. Wang, F. Dai and Z. Li, *Chem. Eng. J.*, 2022, **445**, 136717.
129 J. Ju, L. Hao, S. Yang, D. Wang, Y. Zhang, H. Yuan, X. Yin and Y. Tan, *Adv. Funct. Mater.*, 2020, **30**, 2006544.
130 S. Cheng, Z. Lou, L. Zhang, H. Guo, Z. Wang, C. Guo, K. Fukuda, S. Ma, G. Wang, T. Someya, H.-M. Cheng and X. Xu, *Adv. Mater.*, 2022, 2206793.
131 B. Zhong, K. Jiang, L. Wang and G. Shen, *Adv. Sci.*, 2022, **9**, 2103257.
132 Z. Ma, Q. Huang, Q. Xu, Q. Zhuang, X. Zhao, Y. Yang, H. Qiu, Z. Yang, C. Wang, Y. Chai and Z. Zheng, *Nat. Mater.*, 2021, **20**, 859–868.
133 S. Chen, K. Hou, T. Li, X. Wu, Z. Wang, L. Wei and W. L. Leong, *Adv. Mater. Technol.*, 2022, 2200611.
134 X. He, J. Shi, Y. Hao, M. He, J. Cai, X. Qin, L. Wang and J. Yu, *Carbon Energy*, 2022, **4**, 621–632.
135 H. Li, Z. Wang, M. Sun, H. Zhu, H. Liu, C. Y. Tang and L. Xu, *Adv. Funct. Mater.*, 2022, **32**, 2202792.
136 H. Li, Z. Wang, M. Sun, H. Zhu, H. Liu, C. Y. Tang and L. Xu, *Adv. Funct. Mater.*, 2022, **32**, 2202792.
137 J. Y. Oh and Z. Bao, *Adv. Sci.*, 2019, **6**, 1900186.
138 H. Wu, G. Yang, K. Zhu, S. Liu, W. Guo, Z. Jiang and Z. Li, *Adv. Sci.*, 2020, **8**, 2001938.
139 C. Wang, K. Xia, Y. Zhang and D. L. Kaplan, *Acc. Chem. Res.*, 2019, **52**, 2916–2927.
140 C. Ye, J. Ren, Y. Wang, W. Zhang, C. Qian, J. Han, C. Zhang, K. Jin, M. J. Buehler, D. L. Kaplan and S. Ling, *Matter*, 2019, **1**, 1411–1425.
141 C. E. Campiglio, N. Contessi Negrini, S. Farè and L. Draghi, *Materials*, 2019, **12**, 2476.
142 C. Gao, S. Yuan, K. Cui, Z. Qiu, S. Ge, B. Cao and J. Yu, *Sol. RRL*, 2018, **2**, 1800175.
143 D. Zhao, Y. Zhu, W. Cheng, W. Chen, Y. Wu and H. Yu, *Adv. Mater.*, 2021, **33**, 2000619.
144 M.-S. Hong, G.-M. Choi, J. Kim, J. Jang, B. Choi, J.-K. Kim, S. Jeong, S. Leem, H.-Y. Kwon, H.-B. Hwang, H.-G. Im, J.-U. Park, B.-S. Bae and J. Jin, *Adv. Funct. Mater.*, 2018, **28**, 1705480.
145 X. Wu, H. Liao, D. Ma, M. Chao, Y. Wang, X. Jia, P. Wan and L. Zhang, *J. Mater. Chem. C*, 2020, **8**, 1788–1795.
146 M. Chao, L. He, M. Gong, N. Li, X. Li, L. Peng, F. Shi, L. Zhang and P. Wan, *ACS Nano*, 2021, **15**, 9746–9758.
147 X. Yan, S. Chen, G. Zhang, W. Shi, Z. Peng, Z. Liu, Y. Chen, Y. Huang and L. Liu, *Compos. Sci. Technol.*, 2022, **230**, 109751.
148 J. A. Chiong, H. Tran, Y. Lin, Y. Zheng and Z. Bao, *Adv. Sci.*, 2021, **8**, 2101233.
149 E. Ostroff, K. Parekh, A. Prominski and B. Tian, *Adv. Mater. Technol.*, 2022, **7**, 2100216.
150 Y. Wang, S. Sun and P. Wu, *Adv. Funct. Mater.*, 2021, **31**, 2101494.
151 K. Yamagishi, S. Takeoka and T. Fujie, *Biomater. Sci.*, 2019, **7**, 520–531.
152 Y. Wang, T. Yokota and T. Someya, *NPG Asia Mater.*, 2021, **13**, 22.

 This journal is © The Royal Society of Chemistry 2023

Published on 03 oajagemánnu 2023. Downloaded on 2026-05-06 16:33:29.

153 X. Yang, L. Li, S. Wang, Q. Lu, Y. Bai, F. Sun, T. Li, Y. Li, Z. Wang, Y. Zhao, Y. Shi and T. Zhang, *Adv. Electron. Mater.*, 2020, **6**, 2000306.
154 Q. Duan and Y. Lu, *ACS Appl. Mater. Interfaces*, 2021, **13**, 28832–28842.
155 Y. Liu, Q. Wang, X. Liu, P. Nakielski, F. Pierini, X. Li, J. Yu and B. Ding, *ACS Appl. Bio Mater.*, 2022, **5**, 1047–1056.
156 W. Liu, R. Xie, J. Zhu, J. Wu, J. Hui, X. Zheng, F. Huo and D. Fan, *npj Flexible Electron.*, 2022, **6**, 68.
157 M. Zhou, F. Xu, L. Ma, Q. Luo, W. Ma, R. Wang, C. Lan, X. Pu and X. Qin, *Nano Energy*, 2022, **104**, 107885.
158 T. Zhou, J.-W. Wang, M. Huang, R. An, H. Tan, H. Wei, Z.-D. Chen, X. Wang, X. Liu, F. Wang and J. He, *Small*, 2019, **15**, 1901079.
159 J. T. Reeder, J. Choi, Y. Xue, P. Gutruf, J. Hanson, M. Liu, T. Ray, A. J. Bandodkar, R. Avila, W. Xia, S. Krishnan, S. Xu, K. Barnes, M. Pahnke, R. Ghaffari, Y. Huang and J. A. Rogers, *Sci. Adv.*, 2019, **5**, eaau6356.
160 J. Wang, G. Cai, S. Li, D. Gao, J. Xiong and P. S. Lee, *Adv. Mater.*, 2018, **30**, 1706157.
161 H. Wang, M. Totaro and L. Beccai, *Adv. Sci.*, 2018, **5**, 1800541.
162 Z. Liu, T. Zhu, J. Wang, Z. Zheng, Y. Li, J. Li and Y. Lai, *Nano-Micro Lett.*, 2022, **14**, 61.
163 N. Matsuhisa, X. Chen, Z. Bao and T. Someya, *Chem. Soc. Rev.*, 2019, **48**, 2946–2966.
164 H. Zhao, R. Su, L. Teng, Q. Tian, F. Han, H. Li, Z. Cao, R. Xie, G. Li, X. Liu and Z. Liu, *Nanoscale*, 2022, **14**, 1653–1669.
165 X. Ma, M. Zhang, J. Zhang, S. Wang, S. Cao, Y. Li, G. Hu and D. Kong, *ACS Mater. Lett.*, 2022, **4**, 634–641.
166 W. Wang, S. Yang, K. Ding, L. Jiao, J. Yan, W. Zhao, Y. Ma, T. Wang, B. Cheng and Y. Ni, *Chem. Eng. J.*, 2021, **425**, 129949.
167 Q. Lyu, S. Gong, J. Yin, J. M. Dyson and W. Cheng, *Adv. Healthcare Mater.*, 2021, **10**, 2100577.
168 M. Xu, H. Cai, Z. Liu, F. Chen, Y. Wang, F. Dai and Z. Li, *Int. J. Biol. Macromol.*, 2022, **194**, 755–762.
169 R. Xu, M. She, J. Liu, S. Zhao, H. Liu, L. Qu and M. Tian, *Adv. Fiber Mater.*, 2022, **4**, 1525–1534.
170 X. Peng, K. Dong, C. Ye, Y. Jiang, S. Zhai, R. Cheng, D. Liu, X. Gao, J. Wang and Z. L. Wang, *Sci. Adv.*, 2020, **6**, eaba9624.
171 H. Yeon, H. Lee, Y. Kim, D. Lee, Y. Lee, J.-S. Lee, J. Shin, C. Choi, J.-H. Kang and J. M. Suh, *Sci. Adv.*, 2021, **7**, eabg8459.
172 Y. Wang, H. Haick, S. Guo, C. Wang, S. Lee, T. Yokota and T. Someya, *Chem. Soc. Rev.*, 2022, **51**, 3759–3793.
173 R. He, H. Liu, Y. Niu, H. Zhang, G. M. Genin and F. Xu, *npj Flexible Electron.*, 2022, **6**, 1–11.
174 L.-W. Lo, J. Zhao, K. Aono, W. Li, Z. Wen, S. Pizzella, Y. Wang, S. Chakrabartty and C. Wang, *ACS Nano*, 2022, **16**, 11792–11801.
175 R. He, H. Liu, Y. Niu, H. Zhang, G. M. Genin and F. Xu, *npj Flexible Electron.*, 2022, **6**, 20.
176 H. Yeon, H. Lee, Y. Kim, D. Lee, Y. Lee, J.-S. Lee, J. Shin, C. Choi, J.-H. Kang, J. M. Suh, H. Kim, H. S. Kum, J. Lee, D. Kim, K. Ko, B. S. Ma, P. Lin, S. Han, S. Kim, S.-H. Bae, T.-S. Kim, M.-C. Park, Y.-C. Joo, E. Kim, J. Han and J. Kim, *Sci. Adv.*, 2021, **7**, eabg8459.
177 M. Sharifuzzaman, M. A. Zahed, S. Sharma, S. M. S. Rana, A. Chhetry, Y. D. Shin, M. Asaduzzaman, S. Zhang, S. Yoon, X. Hui, H. Yoon and J. Y. Park, *Adv. Funct. Mater.*, 2021, **32**, 2107969.
178 J. Xu, X. Li, H. Chang, B. Zhao, X. Tan, Y. Yang, H. Tian, S. Zhang and T.-L. Ren, *ACS Nano*, 2022, **16**, 6687–6699.
179 M. O. G. Nayeem, S. Lee, H. Jin, N. Matsuhisa, H. Jinno, A. Miyamoto, T. Yokota and T. Someya, *Proc. Natl. Acad. Sci. U. S. A.*, 2020, **117**, 7063–7070.
180 X. Niu, X. Gao, Y. Liu and H. Liu, *Measurement*, 2021, **183**, 109774.
181 W. Hwang, J. Kim, S. Park, T. H. Kang, S. Kim, K. Lee, M. G. Lee, R. Kwak, I. S. Choi and H. Yi, *Adv. Mater. Technol.*, 2022, 2200477, DOI: **10.1002/admt.202200477**.
182 S. Yu, Y. Tai, J. Milam-Guerrero, J. Nam and N. V. Myung, *Nano Energy*, 2022, **97**, 107174.
183 S. Chen, J. Qi, S. Fan, Z. Qiao, J. C. Yeo and C. T. Lim, *Adv. Healthcare Mater.*, 2021, **10**, 2100116.
184 S. H. Kwon and L. Dong, *Nano Energy*, 2022, **102**, 107632.
185 D. W. Kim, M. Kong and U. Jeong, *Adv. Sci.*, 2021, **8**, 2004170.
186 A. S. Farooq and P. Zhang, *Sens. Actuators, A*, 2022, **344**, 113715.
187 W. Jeong, J. Song, J. Bae, K. R. Nandanapalli and S. Lee, *ACS Appl. Mater. Interfaces*, 2019, **11**, 44758–44763.
188 J. H. Koo, J.-K. Song, S. Yoo, S.-H. Sunwoo, D. Son and D.-H. Kim, *Adv. Mater. Technol.*, 2020, **5**, 2000407.
189 H. Liu, L. Wang, G. Lin and Y. Feng, *Biomater. Sci.*, 2022, **10**, 614–632.
190 C. Okutani, T. Yokota and T. Someya, *Adv. Sci.*, 2022, 2202312, DOI: **10.1002/advs.202202312**.
191 M. Gong, P. Wan, D. Ma, M. Zhong, M. Liao, J. Ye, R. Shi and L. Zhang, *Adv. Funct. Mater.*, 2019, **29**, 1902127.
192 Q. Li, L. N. Zhang, X. M. Tao and X. Ding, *Adv. Healthcare Mater.*, 2017, **6**, 1601371.
193 J. Huang, Z. Xu, W. Qiu, F. Chen, Z. Meng, C. Hou, W. Guo and X. Y. Liu, *Adv. Funct. Mater.*, 2020, **30**, 1910547.
194 H. Zhang, R. He, H. Liu, Y. Niu, Z. Li, F. Han, J. Li, X. Zhang and F. Xu, *Sens. Actuators, A*, 2021, **322**, 112611.
195 W. Jeong, S. Lee, S. Yoo, S. Park, H. Choi, J. Bae, Y. Lee, K. Woo, J.-H. Choi and S. Lee, *ACS Appl. Mater. Interfaces*, 2021, **13**, 60425–60432.
196 H. Li, Z. Wang, M. Sun, H. Zhu, H. Liu, C. Y. Tang and L. Xu, *Adv. Funct. Mater.*, 2022, 2202792, DOI: **10.1002/adfm.202202792**.
197 Z. Cui, F. R. Poblete and Y. Zhu, *ACS Appl. Mater. Interfaces*, 2019, **11**, 17836–17842.
198 S. Sang, Z. Pei, F. Zhang, C. Ji, Q. Li, J. Ji, K. Yang and Q. Zhang, *ACS Appl. Mater. Interfaces*, 2022, **14**, 31493–31501.

Published on 03 oajagemánnu 2023. Downloaded on 2026-05-06 16:33:29.

199 O. Yue, X. Wang, X. Liu, M. Hou, M. Zheng, Y. Wang and B. Cui, *Adv. Sci.*, 2021, **8**, 2004377.
200 Y. Xu, B. Sun, Y. Ling, Q. Fei, Z. Chen, X. Li, P. Guo, N. Jeon, S. Goswami, Y. Liao, S. Ding, Q. Yu, J. Lin, G. Huang and Z. Yan, *Proc. Natl. Acad. Sci. U. S. A.*, 2020, **117**, 205–213.
201 M. Li, J. Chen, W. Zhong, M. Luo, W. Wang, X. Qing, Y. Lu, Q. Liu, K. Liu, Y. Wang and D. Wang, *ACS Sens.*, 2020, **5**, 2545–2554.
202 I. Wicaksono, C. I. Tucker, T. Sun, C. A. Guerrero, C. Liu, W. M. Woo, E. J. Pence and C. Dagdeviren, *npj Flexible Electron.*, 2020, **4**, 1–13.
203 Z. Ouyang, S. Cui, H. Yu, D. Xu, C. Wang, D. Tang and K. C. Tam, *Nano Res.*, 2021, **15**, 1027–1038.
204 J. Luo, S. Gao, H. Luo, L. Wang, X. Huang, Z. Guo, X. Lai, L. Lin, R. K. Y. Li and J. Gao, *Chem. Eng. J.*, 2021, **406**, 126898.
205 T. H. Park, S. Park, S. Yu, S. Park, J. Lee, S. Kim, Y. Jung and H. Yi, *Adv. Healthcare Mater.*, 2021, **10**, 2100469.
206 M. Sang, K. Kang, Y. Zhang, H. Zhang, K. Kim, M. Cho, J. Shin, J.-H. Hong, T. Kim, S. K. Lee, W.-H. Yeo, J. W. Lee, T. Lee, B. Xu and K. J. Yu, *Adv. Mater.*, 2022, **34**, 2105865.
207 J. Shin, B. Jeong, J. Kim, V. B. Nam, Y. Yoon, J. Jung, S. Hong, H. Lee, H. Eom, J. Yeo, J. Choi, D. Lee and S. H. Ko, *Adv. Mater.*, 2020, **32**, 1905527.
208 Y. Yu, G. Zheng, K. Dai, W. Zhai, K. Zhou, Y. Jia, G. Zheng, Z. Zhang, C. Liu and C. Shen, *Mater. Horiz.*, 2021, **8**, 1037–1046.
209 J. Zhou, Z. Zhao, R. Hu, J. Yang, H. Xiao, Y. Liu and M. Lu, *Mater. Des.*, 2020, **191**, 108636.
210 T. Delipinar, A. Shafique, M. S. Gohar and M. K. Yapici, *ACS Omega*, 2021, **6**, 8744–8753.
211 T. Li, L. Li, H. Sun, Y. Xu, X. Wang, H. Luo, Z. Liu and T. Zhang, *Adv. Sci.*, 2017, **4**, 1600404.
212 J. Wu, Z. Wu, K. Tao, C. Liu, B.-R. Yang, X. Xie and X. Lu, *J. Mater. Chem. B*, 2019, **7**, 2063–2073.
213 Z. Li, J. Wang, Y. Xu, M. Shen, C. Duan, L. Dai and Y. Ni, *Carbohydr. Polym.*, 2021, **270**, 118385.
214 Y. Wang, Y. Zhou and Y. Wang, *Sens. Actuators, B*, 2020, **323**, 128695.
215 M. A. Najeeb, Z. Ahmad and R. A. Shakoor, *Adv. Mater. Interfaces*, 2018, **5**, 1800969.
216 Y. Lu, G. Yang, Y. Shen, H. Yang and K. Xu, *Nano-Micro Lett.*, 2022, **14**, 150.
217 N. Pal, *Adv. Colloid Interface Sci.*, 2020, **280**, 102156.
218 Z. Ouyang, S. Cui, H. Yu, D. Xu, C. Wang, D. Tang and K. C. Tam, *Nano Res.*, 2022, **15**, 1027–1038.
219 Y. Niu, H. Liu, R. He, Z. Li, H. Ren, B. Gao, H. Guo, G. M. Genin and F. Xu, *Mater. Today*, 2020, **41**, 219–242.
220 Y. Xu, B. Sun, Y. Ling, Q. Fei, Z. Chen, X. Li, P. Guo, N. Jeon, S. Goswami and Y. Liao, *Proc. Natl. Acad. Sci. U. S. A.*, 2020, **117**, 205–213.
221 H. Li, Y. Ma and Y. Huang, *Mater. Horiz.*, 2021, **8**, 383–400.
222 Y. Pang, X. Xu, S. Chen, Y. Fang, X. Shi, Y. Deng, Z.-L. Wang and C. Cao, *Nano Energy*, 2022, **96**, 107137.
223 S. Li, Y. Zhang, Y. Wang, K. Xia, Z. Yin, H. Wang, M. Zhang, X. Liang, H. Lu, M. Zhu, H. Wang, X. Shen and Y. Zhang, *InfoMat*, 2020, **2**, 184–211.
224 M. Zhu, H. Wang, S. Li, X. Liang, M. Zhang, X. Dai and Y. Zhang, *Adv. Healthcare Mater.*, 2021, **10**, 2100646.
225 C. Ma, M. Wang, P. C. Uzabakiriho and G. Zhao, *Adv. Mater. Technol.*, 2022, 2200106, DOI: **10.1002/admt.202200106**.
226 C. Wang, X. Li, E. Gao, M. Jian, K. Xia, Q. Wang, Z. Xu, T. Ren and Y. Zhang, *Adv. Mater.*, 2016, **28**, 6640–6648.
227 M. Fu, J. Zhang, Y. Jin, Y. Zhao, S. Huang and C. F. Guo, *Adv. Sci.*, 2020, **7**, 2000258.
228 S. R. A. Ruth, V. R. Feig, H. Tran and Z. Bao, *Adv. Funct. Mater.*, 2020, **30**, 2003491.
229 X. Yu, X. Wu, Y. Si, X. Wang, J. Yu and B. Ding, *Macromol. Rapid Commun.*, 2019, **40**, 1800931.
230 W. Yang, N.-W. Li, S. Zhao, Z. Yuan, J. Wang, X. Du, B. Wang, R. Cao, X. Li, W. Xu, Z. L. Wang and C. Li, *Adv. Mater. Technol.*, 2017, **3**, 1700241.
231 W. Chen and X. Yan, *J. Mater. Sci. Technol.*, 2020, **43**, 175–188.
232 Y. Luo, L. Zhao, G. Luo, M. Li, X. Han, Y. Xia, Z. Li, Q. Lin, P. Yang, L. Dai, G. Niu, X. Wang, J. Wang, D. Lu and Z. Jiang, *Nanotechnology*, 2022, **33**, 415502.
233 Z. Liu, K. Chen, A. Fernando, Y. Gao, G. Li, L. Jin, H. Zhai, Y. Yi, L. Xu, Y. Zheng, H. Li, Y. Fan, Y. Li and Z. Zheng, *Chem. Eng. J.*, 2021, **403**, 126191.
234 Z. Zhao, Q. Huang, C. Yan, Y. Liu, X. Zeng, X. Wei, Y. Hu and Z. Zheng, *Nano Energy*, 2020, **70**, 104528.
235 X. Zheng, Q. Hu, Z. Wang, W. Nie, P. Wang and C. Li, *J. Colloid Interface Sci.*, 2021, **602**, 680–688.
236 Z. Li, M. Zhu, J. Shen, Q. Qiu, J. Yu and B. Ding, *Adv. Funct. Mater.*, 2020, **30**, 1908411.
237 M. Lei, K. Feng, S. Ding, M. Wang, Z. Dai, R. Liu, Y. Gao, Y. Zhou, Q. Xu and B. Zhou, *ACS Nano*, 2022, **8**, 12620–12634.
238 L. Yuan, M. Zhang, T. Zhao, T. Li, H. Zhang, L. Chen and J. Zhang, *Sens. Actuators, A*, 2020, **315**, 112192.
239 K. Zhao, W. Niu and S. Zhang, *J. Mater. Sci.*, 2019, **55**, 2439–2453.
240 X. Zhang, L. Ke, X. Zhang, F. Xu, Y. Hu, H. Lin and J. Zhu, *ACS Appl. Mater. Interfaces*, 2022, **14**, 25753–25762.
241 S. Wang, H. Huang, C. Liu, Y. Xia, C. Ye, Z. Luo, C. Cai, C. Wang, L. Lyu, H. Bi, X. Wu and L. Sun, *Adv. Mater. Technol.*, 2022, 2200149, DOI: **10.1002/admt.202200149**.
242 Y.-R. Ding, C.-H. Xue, X.-J. Guo, X. Wang, S.-T. Jia and Q.-F. An, *ACS Appl. Electron. Mater.*, 2022, **4**, 345–355.
243 C. Tan, Z. Dong, Y. Li, H. Zhao, X. Huang, Z. Zhou, J.-W. Jiang, Y.-Z. Long, P. Jiang, T.-Y. Zhang and B. Sun, *Nat. Commun.*, 2020, **11**, 1–10.
244 Y. Liu, Y. Cheng, L. Shi, R. Wang and J. Sun, *ACS Appl. Mater. Interfaces*, 2022, **14**, 12812–12823.
245 Z. Yan, D. Xu, Z. Lin, P. Wang, B. Cao, H. Ren, F. Song, C. Wan, L. Wang, J. Zhou, X. Zhao, J. Chen, Y. Huang and X. Duan, *Science*, 2022, **375**, 852–859.
246 H. Liu, Y. Ni, J. Hu, Y. Jin, P. Gu, H. Qiu and K. Chen, *ACS Appl. Mater. Interfaces*, 2022, **14**, 21509–21520.

 This journal is © The Royal Society of Chemistry 2023

Published on 03 oajagemännu 2023. Downloaded on 2026-05-06 16:33:29.

247 X. Lin, Y. Bing, F. Li, H. Mei, S. Liu, T. Fei, H. Zhao and T. Zhang, *Adv. Mater. Technol.*, 2022, **7**, 2101312.
248 X. Cui, J. Chen, W. Wu, Y. Liu, H. Li, Z. Xu and Y. Zhu, *Nano Energy*, 2022, **95**, 107022.
249 M. Chao, L. He, M. Gong, N. Li, X. Li, L. Peng, F. Shi, L. Zhang and P. Wan, *ACS Nano*, 2021, **15**, 9746–9758.
250 J. Xiang, R. Yu, L. Yang, P. Zhao, R. Wang, X. Wu, B. Peng and G. Liu, *ACS Appl. Mater. Interfaces*, 2022, **14**, 21645–21656.
251 Y. Wang, M. Chao, P. Wan and L. Zhang, *Nano Energy*, 2020, **70**, 104560.
252 M. Xu, H. Cai, Z. Liu, F. Chen, L. Chen, X. Chen, X. Cheng, F. Dai and Z. Li, *Adv. Electron. Mater.*, 2021, **7**, 2100368.
253 J. Wang, Y. Lou, B. Wang, Q. Sun, M. Zhou and X. Li, *Sensors*, 2020, **20**, 2459.
254 L. Ke, Y. Wang, X. Ye, W. Luo, X. Huang and B. Shi, *J. Mater. Chem. C*, 2019, **7**, 2548–2556.
255 S. Han, Q. Wan, K. Zhou, A. Yan, Z. Lin, B. Shu and C. Liu, *ACS Appl. Nano Mater.*, 2021, **4**, 8273–8281.
256 M. Fu, J. Zhang, Y. Jin, Y. Zhao, S. Huang and C. F. Guo, *Adv. Sci.*, 2020, **7**, 2000258.
257 B. Shi, Z. Li and Y. Fan, *Adv. Mater.*, 2018, **30**, 1801511.
258 S. Hadke, M. Huang, C. Chen, Y. F. Tay, S. Chen, J. Tang and L. Wong, *Chem. Rev.*, 2022, **122**, 10170–10265.
259 N. Sun, G.-G. Wang, H.-X. Zhao, Y.-W. Cai, J.-Z. Li, G.-Z. Li, X.-N. Zhang, B.-L. Wang, J.-C. Han and Y. Wang, *Nano Energy*, 2021, **90**, 106639.
260 K. Zhou, Y. Zhao, X. Sun, Z. Yuan, G. Zheng, K. Dai, L. Mi, C. Pan, C. Liu and C. Shen, *Nano Energy*, 2020, **70**, 104546.
261 M. Sala de Medeiros, D. Chanci, C. Moreno, D. Goswami and R. V. Martinez, *Adv. Funct. Mater.*, 2019, **29**, 1904350.
262 X. Guan, B. Xu, M. Wu, T. Jing, Y. Yang and Y. Gao, *Nano Energy*, 2021, **80**, 105549.
263 Q. Qiu, M. Zhu, Z. Li, K. Qiu, X. Liu, J. Yu and B. Ding, *Nano Energy*, 2019, **58**, 750–758.
264 W. Yang, R. Cao, X. Zhang, H. Li and C. Li, *Adv. Mater. Technol.*, 2018, **3**, 1800178.
265 C. Wu, A. C. Wang, W. Ding, H. Guo and Z. L. Wang, *Adv. Energy Mater.*, 2019, **9**, 1802906.
266 Y. Wang, Y. Yang and Z. L. Wang, *npj Flexible Electron.*, 2017, **1**, 1–10.
267 Z. L. Wang and J. Song, *Science*, 2006, **312**, 242–246.
268 J.-a. Li, Z. Ma, H.-t. Wang, X.-x. Gao, Z. Zhou, R.-w. Tao, L.-j. Pan and Y. Shi, *Adv. Intell. Syst.*, 2019, **1**, 1900063.
269 M. Pan, C. Yuan, X. Liang, J. Zou, Y. Zhang and C. Bowen, *iScience*, 2020, **23**, 101682.
270 Y. Shi, X. Wei, K. Wang, D. He, Z. Yuan, J. Xu, Z. Wu and Z. L. Wang, *ACS Appl. Mater. Interfaces*, 2021, **13**, 50329–50337.
271 Z. Li, M. Zhu, Q. Qiu, J. Yu and B. Ding, *Nano Energy*, 2018, **53**, 726–733.
272 Y. Hu and Z. Zheng, *Nano Energy*, 2019, **56**, 16–24.
273 J. S. Chae, S. K. Park, K. C. Roh and H. S. Park, *Energy Storage Mater.*, 2020, **24**, 113–128.
274 M. Hassan, G. Abbas, N. Li, A. Afzal, Z. Haider, S. Ahmed, X. Xu, C. Pan and Z. Peng, *Adv. Mater. Technol.*, 2022, **7**, 2100773.
275 W. Yang and X. Lu, *Adv. Mater. Technol.*, 2019, **4**, 1900745.
276 Y. Liu, X. Huang, J. Zhou, J. Li, S. K. Nejad, C. K. Yiu, H. Li, T. H. Wong, W. Park, K. Yao, L. Zhao, R. Shi, Y. Wang, Z. Dai and X. Yu, *Nano Energy*, 2022, **92**, 106755.
277 J. Yin, W. Zhang, N. A. Alhebshi, N. Salah and H. N. Alshareef, *Small Methods*, 2020, **4**, 1900853.
278 M. Kandasamy, S. Sahoo, S. K. Nayak, B. Chakraborty and C. S. Rout, *J. Mater. Chem. A*, 2021, **9**, 17643–17700.
279 Z. Lin, M. Mao, J. Yue, B. Liu, C. Wu, L. Suo, Y.-S. Hu, H. Li, X. Huang and L. Chen, *ACS Mater. Lett.*, 2020, **2**, 808–813.
280 J. Chang, J. Shang, Y. Sun, L. K. Ono, D. Wang, Z. Ma, Q. Huang, D. Chen, G. Liu and Y. Cui, *Nat. Commun.*, 2018, **9**, 1–11.
281 J. He, C. Lu, H. Jiang, F. Han, X. Shi, J. Wu, L. Wang, T. Chen, J. Wang, Y. Zhang, H. Yang, G. Zhang, X. Sun, B. Wang, P. Chen, Y. Wang, Y. Xia and H. Peng, *Nature*, 2021, **597**, 57–63.
282 Z. Liu, H. Li, M. Zhu, Y. Huang, Z. Tang, Z. Pei, Z. Wang, Z. Shi, J. Liu, Y. Huang and C. Zhi, *Nano Energy*, 2018, **44**, 164–173.
283 H. Song, S. Xu, Y. Li, J. Dai, A. Gong, M. Zhu, C. Zhu, C. Chen, Y. Chen, Y. Yao, B. Liu, J. Song, G. Pastel and L. Hu, *Adv. Energy Mater.*, 2018, **8**, 1701203.
284 Y. Liu, X. Huang, J. Zhou, C. K. Yiu, Z. Song, W. Huang, S. K. Nejad, H. Li, T. H. Wong and K. Yao, *Adv. Sci.*, 2022, **9**, 2104635.
285 X. Huang, Y. Liu, J. Zhou, S. K. Nejad, T. H. Wong, Y. Huang, H. Li, C. K. Yiu, W. Park and J. Li, *npj Flexible Electron.*, 2022, **6**, 1–8.
286 X. Lin, J. Wang, X. Gao, S. Wang, Q. Sun, J. Luo, C. Zhao, Y. Zhao, X. Yang, C. Wang, R. Li and X. Sun, *Chem. Mater.*, 2020, **32**, 3018–3027.
287 H. Wang, Y. Jiao, S. Wang, P. Ye, J. Ning, Y. Zhong and Y. Hu, *Small*, 2021, **17**, 2103517.
288 J. Wu, L. Hu, N. Wang, Y. Li, D. Zhao, L. Li, X. Peng, Z. Cui, L.-J. Ma, Y. Tian and X. Wang, *Appl. Catal., B*, 2019, **254**, 55–65.
289 W. Wang, C. Xiang, Q. Liu, M. Li, W. Zhong, K. Yan and D. Wang, *J. Mater. Chem. A*, 2018, **6**, 22599–22608.
290 C. Xiang, J. Guo, R. Sun, A. Hinitt, T. Helps, M. Taghavi and J. Rossiter, *Polymers*, 2019, **11**, 1199.
291 X. Yu, Z. Xie, Y. Yu, J. Lee, A. Vazquez-Guardado, H. Luan, J. Ruban, X. Ning, A. Akhtar and D. Li, *Nature*, 2019, **575**, 473–479.
292 J. Heikenfeld, A. Jajack, B. Feldman, S. W. Granger, S. Gaitonde, G. Begtrup and B. A. Katchman, *Nat. Biotechnol.*, 2019, **37**, 407–419.
293 Y. Yu, H. Y. Y. Nyein, W. Gao and A. Javey, *Adv. Mater.*, 2020, **32**, 1902083.
294 M. Ghoneim, A. Nguyen, N. Dereje, J. Huang, G. Moore, P. Murzynowski and C. Dagdeviren, *Chem. Rev.*, 2019, **119**, 5248–5297.

295 J. Zhang, G. Jiang, T. Cumberland, P. Xu, Y. Wu, S. Delaat, A. Yu and Z. Chen, *InfoMat*, 2019, **1**, 234–241.
296 Y. L. Li, Y. H. Liu, L. S. Chen and J. L. Xu, *Adv. Healthcare Mater.*, 2021, **10**, 2100046.
297 H. Wang, S. Li, Y. Wang, H. Wang, X. Shen, M. Zhang, H. Lu, M. He and Y. Zhang, *Adv. Mater.*, 2020, **32**, 1908214.
298 T. An, Y. Ling, S. Gong, B. Zhu, Y. Zhao, D. Dong, L. W. Yap, Y. Wang and W. Cheng, *Adv. Mater. Technol.*, 2019, **4**, 1800473.
299 S. Gong, L. W. Yap, Y. Zhu, B. Zhu, Y. Wang, Y. Ling, Y. Zhao, T. An, Y. Lu and W. Cheng, *Adv. Funct. Mater.*, 2020, **30**, 1910717.
300 X. Lin, F. Li, Y. Bing, T. Fei, S. Liu, H. Zhao and T. Zhang, *Nano-Micro Lett.*, 2021, **13**, 1–14.
301 H. Kim, S. Park, I. G. Jeong, S. H. Song, Y. Jeong, C.-S. Kim and K. H. Lee, *ACS Nano*, 2021, **15**, 4054–4065.
302 M. A. Makroum, M. Adda, A. Bouzouane and H. Ibrahim, *Sensors*, 2022, **22**, 1843.
303 B. Shan, Y. Y. Broza, W. Li, Y. Wang, S. Wu, Z. Liu, J. Wang, S. Gui, L. Wang, Z. Zhang, W. Liu, S. Zhou, W. Jin, Q. Zhang, D. Hu, L. Lin, Q. Zhang, W. Li, J. Wang, H. Liu, Y. Pan and H. Haick, *ACS Nano*, 2020, **14**, 12125–12132.
304 H. Haick and N. Tang, *ACS Nano*, 2021, **15**, 3557–3567.
305 Y. Zheng, N. Tang, R. Omar, Z. Hu, T. Duong, J. Wang, W. Wu and H. Haick, *Adv. Funct. Mater.*, 2021, **31**, 2105482.

Published on 03 oajagemánnu 2023. Downloaded on 2026-05-06 16:33:29.


This journal is © The Royal Society of Chemistry 2023